HuPSA and MoPSA Atlases Revealed Novel Cell Populations and Lineage Plasticity in Prostate Cancer at Single-Cell Level

Siyuan Cheng[1,2], Lin Li[1,2], Yingli Shi[1,2], Xiuping Yu[1,2,3]

1. Department of Biochemistry and Molecular biology, LSU Health Shreveport, Shreveport, LA

2. Feist-Weiller Cancer Center, LSU Health Shreveport, Shreveport, LA

3. Department of Urology, LSU Health Shreveport, Shreveport, LA

Correspondence to S. Cheng and X. Yu

Abstract

Androgen deprivation therapy has improved patient survival. Nevertheless, treatment resistance inevitably emerges due to the complex interplay of tumor heterogeneity and lineage plasticity. We integrated scRNAseq data from multiple studies, including both public cohorts and data generated in our laboratory, and generated the HuPSA (Human Prostate Single cell Atlas) and MoPSA (Mouse Prostate Single cell Atlas) datasets. Through unsupervised clustering and manual annotation, we found that both atlases consisted of previously known cell clusters including prostate adenocarcinoma (AdPCa), neuroendocrine prostate cancer (NEPCa), stromal, and immune cell populations. Our analysis also unearthed the less described populations including MMP7^{+} normal prostate club cells and two novel lineage plastic cancerous populations, namely progenitor-like and KRT7^{+} cells. Immunohistochemical staining analysis confirmed the presence of these populations in both human and mouse PCa tissues, reinforcing their significance in PCa pathobiology. To unravel the molecular drivers of these distinct cell populations, we explored the upstream regulators of the genes enriched in these cells and found that Wnt signaling is enriched in these progenitor-like cells. Furthermore, employing HuPSA-based deconvolution, we scrutinized over one thousand human PCa bulk RNAseq samples and reclassified them into different molecular subtypes, including the newly discovered KRT7 and progenitor-like categories. Moreover, employing supervised dimensional reduction and label transferring techniques, we mapped the scRNAseq data derived from C4-2B xenograft tumors onto HuPSA. Our analysis effectively unveiled the populational heterogeneity and neuroendocrine differentiation in this C4-2B xenograft model. In conclusion, our study elucidates a roadmap of PCa progression, showcasing the development of heterogeneous populations through lineage plasticity. This understanding holds promise for guiding the development of precise medicine in PCa field. Additionally, the HuPSA and MoPSA provide invaluable blueprints for analyzing and interpreting external PCa single-cell RNAseq data.

Introduction

Prostate cancer (PCa) represents a significant public health challenge in the United States, being the most commonly diagnosed cancer among men[1]. Although various treatments including anti-androgen drugs and androgen synthesis inhibitors have been employed, these treatments eventually fail, leading to the progression of the cancer into a "castration-resistant" stage. In this stage, cancer cells acquire the ability to proliferate independently of androgen stimulation[2]. A subset of castration-resistant prostate cancer (CRPCa) cases retain the characteristics of prostate adenocarcinoma (AdPCa), expressing the markers associated with the luminal epithelia of the prostate, such as AR, AR targets, and HOXB13[3,4]. Another portion of CRPCa cases, approximately 30%, presents an alternative phenotype known as

neuroendocrine prostate cancer (NEPCa). NEPCa cells express low or absent levels of the androgen receptor (AR) and its downstream genes, while expressing high levels of neuroendocrine markers such as CHGA and NCAM1 (CD56). [5] In addition to the aforementioned phenotypes, there exists a lesser studied phenotype known as double negative prostate cancer (DNPCa), characterized by the absence of both luminal and neuroendocrine features[6,7].

Lineage plasticity is implicated in the transition of AdPCa to NEPCa and DNPCa. Lineage plasticity is a phenomenon where tumor cells undergo changes in their morphology and functions to adapt to stressful conditions or environmental pressures. This dynamic process enables cells to transit to different cellular states[8]. In our previous study, we have developed a method to quantify the lineage plasticity by calculating the Pearson correlation between the expression of all 39 HOX genes in samples and the prostatic HOX code derived from human prostate cancer (PCa) cell lines[4]. We have shown that the prostatic lineage feature represented by "HOX code" or the expression of HOXB13 is reduced or lost in NEPCa[4]. Additionally, previous studies have shown that SOX2, SRRM4, ONECUT2, BRN2, PEG10, Jak-stat signaling can contribute to PCa lineage plasticity[7,9-13].

Single-cell RNA sequencing (scRNAseq) is a powerful tool to study the heterogenous cell types in the tumors. This technique has been used in multiple studies to explore the progression path of lineage plasticity and the spectra of cell population heterogeneity in PCa. These investigations have revealed the various cell populations in human prostatic samples, including AdPCa, NEPCa, luminal and basal epithelia, club, stromal, and immune cells. In mouse samples, AdPCa, NEPCa, luminal and basal epithelia populations have also been identified as well as some rare Foxi1^{+}, Pou2f3^{+} cells [7,14-28]. It is noteworthy that certain populations identified in these studies may exhibit inconsistencies across different studies. Moreover, due to the relatively small sample sizes in each individual study, some rare populations might be overlooked. It is also important to exercise caution in the interpretation of cell populations because they might be model-specific.

In the current study, we established two integrated scRNAseq datasets: Human Prostate Single cell Atlas (HuPSA) and Mouse Prostate Single cell Atlas (MoPSA). Leveraging these atlases, we were able to identify and characterize previously undiscovered populations within prostatic tissues.

Results

1. Establishment of HuPSA and MoPSA by compiling single cell RNA sequencing data obtained from multiple studies.

Using publicly available scRNAseq data, we established two combined datasets and visualized the data on UMAP as Human Prostate Single cell Atlas (HuPSA) and Mouse Prostate Single cell Atlas (MoPSA). The HuPSA dataset compiled single cell RNA sequencing data of 73 distinct samples from 6 studies, consisting of 368,831 high-quality cells. Based on their original records, these 73 samples span eight histology groups, namely Normal, Normal adjacent, Benign, AdPCa, CSPCa (castration-sensitive PCa), CRPCa, mCRPCa (metastatic CRPCa), and Cribriform PCa.

For the establishment of MoPSA, because the publicly available mouse prostate scRNAseq datasets lack TRAMP model, a widely utilized mouse model for NEPCa research, we included in the MoPSA dataset TRAMP scRNAseq data that were newly generated by our group. The compiled MoPSA dataset consisted of 395,917 cells originated from 138 samples obtained from 13 studies. These 138 samples

were derived from murine prostatic tissues under different treatment modalities, whereby the samples were classified into six groups including WT (wild-type), GEM (genetically engineered mice), Control (GEM control mice that express tamoxifen-induced YFP in prostate), Castration, Regeneration (androgen -induced prostate regeneration), and Development (developing prostate).

UMAP analysis of the compiled scRNAseq data revealed distinct cell clusters, including stromal, endothelial, multiple epithelial and immune clusters (Fig. 1). Each cluster was further separated into different populations based on their molecular features, resulting in 26 and 21 populations in HuPSA and MoPSA, respectively (sFig. 1). Sankey diagrams, which visualize the data flow between the cell populations and the histology of samples, demonstrated the sample types from which the cells of each population were derived.

Most epithelial clusters (including basal/basal-like, luminal, and NEPCa) were shared between HuPSA amd MoPSA, whereas Progenitor-like cluster only stood out in HuPSA and Pou2f3 cluster was only in MoPSA. The epithelial clusters were further separated into different populations that were defined based on copy-number variation (CNV), expression of marker genes, and recorded sample histology (sFig. 1 & sFig. 2).

2. Luminal cells in HuPSA and MoPSA

In HuPSA, the Luminal cluster expressed HOXB13, FOXA1 and NKX3-1. This cluster consisted of seven populations including Normal (contributed by Normal, Normal-adjacent, Benign, and some AdPCa samples), three groups of AdPCa_AR+ as well as AdPCa_AR high (AR_hi), AdPCa_AR low (AR_lo), and highly_ proliferating groups. The AdPCa_AR+_1 population only slightly deviated from Normal cells on UMAP (Fig. 2). Its inferred copy number variation (CNV) pattern was also similar to Normal cells (sFig.6). This population may represent low grade PCa and cells in this population are still at early stage of transformation. On the contrary, AdPCa_AR+_2 population harbored higher level of copy number variations (sFig. 6). The highest level of CNV was present in the AdPCa_AR_high population, suggesting a genome instability in these cells. The AdPCa_AR+_2 and AR-high populations were mostly derived from advanced PCa samples including CRPC, mCRPC, and CSPC (Fig, 2E). Another population that was mostly derived from advanced PCa samples is AdPCa_AR+_3. It departed from the main body of AdPCa but its inferred CNV pattern did not show much difference from the Normal cells, suggesting that genome instability may not be a driving mechanism in these cells. It is interesting to note that AdPCa_AR+_3 expressed Neuropeptide Y (NPY) as well as two smooth muscle markers (TAGLN and ACTA2). This suggests the AdPCa_AR+_3 population may have acquired certain mesenchymal features while still expressing luminal genes (HOXB13, FOXA1 and NKX3-1) (Fig, 2C&D; sFig1). These cancer cells are likely driven by epigenetic reprogramming.

The AdPCa_AR low population, although low in AR expression, still expressed KLK3 and NKX3-1, two AR target genes, at fair levels, indicating an active AR signaling in these cells.

The proliferating population exhibited high proliferative activity as indicated by the high expression of Ki67 and TOP2A. The cells in this population were mostly derived from CRPC and mCRPC as well as CSPC samples. This population exhibited active AR signaling, indicated by the expression of AR and AR target, KLK3.

The Luminal cluster in MoPSA also contained multiple populations, including LE/AdPCa_1, AdPCa_2 & _3, and highly proliferating populations, as well as a unique Spink1 population that was not detected in HuPSA. The Spink1 population was dominantly contributed by WT mouse tissues (sFig. 2) and harbored low copy number variation (sFig. 6). Because of its absence in HuPSA and the relatively normal molecular profiles, the Spink1 population will not be further characterized in this study.

All the other Luminal cells in MoPSA expressed HOXB13 and FOXA1, like those in HuPSA. But NKX3-1, a prostate differentiation marker, was only expressed in the normal LE/AdPCa_1 population at high level, suggesting a loss of differentiation state in the other populations. The LE/AdPCa_1 population was mostly originated from wild type mice, but GEM samples contributed to this population as well. This populations harbored low copy number variation (sFig. 6); therefore, it may represent normal cells and the cells at early stage of transformation. On the contrary, the other AdPCa populations, including ADPCa_2 & _3, and highly proliferating populations, were predominantly contributed by GEM (sFig. 2) and harbored slightly higher level of CNV than the LE/AdPCa_1 cells (sFig. 6).

In HuPSA, all the Luminal populations expressed KLK3, an AR target gene, regardless of AR's expression status, whereas in MoPSA, only the normal LE/AdPCa_1 population expressed Pbsn, an AR target gene in murine prostate. Its low expression in the rest luminal populations suggests the de-differentiation state of these cells.

3. Basal/basal-like cells in HuPSA and MoPSA

The Basal/basal-like cluster in HuPSA contained three populations including Basal (KRT5+, KRT14+, TP63+), Club (MMP7+, WFDC2+) and KRT7 (KRT7+, S100A9+). The Club and KRT7 populations, although clustered together with basal epithelial cells, express low to no basal markers, suggesting their basal features but not basal identity. In MoPSA, the Basal and Krt7 populations were present as well, but the Club group was not (Fig. 1).

<u>In HuPSA, KRT7 population exhibited a lineage-switched double-negative PCa phenotype.</u>

The KRT7 population in HuPSA was characterized by the high expression of KRT7 and S100A9. Although KRT7 expression was also detected in other three populations including Club, Basal, and NEPCa (sFig. 1 and Fig. 4A), its expression level was relatively lower in these populations. Additionally, their transcription profiles were separate from the KRT7 population. The HuPSA KRT7 population comprised 1937 cells, 1828 of them (94%) were derived from mCRPCa samples. Also, this population exhibited higher levels of copy number variations compared to Normal cells or early AdPCa (sFig. 6). These features suggest that the KRT7 population in HuPSA are cancerous cells but not un-transformed basal cells, which express KRT7 as well, albeit at lower level.

This was further corroborated by the KRT7 protein expression pattern in human prostatic tissues. As shown in Fig. 5A, KRT7 expression was present in the basal epithelia but absent in the luminal epithelia of benign prostatic tissues. Its expression was absent in most AdPCa specimens (Fig. 5B) but scattered or patchy KRT7 expression was detected in some rare cells of advanced AdPCa (Figs. 5C and 5D).

We also assessed KRT7 expression in PCa cell lines and cell line-derived xenografts (Figs. 5E-L). Its expression was detected in two cell lines that represent advanced PCa, PC3 and DU145, as well as some rare cells scattered in the 22RV1 xenograft tumor. The PC3 tumors displayed high KRT7 expression in

some focal areas, whereas DU145 tumors expressed moderate Krt7 throughout the tissue. In contrast, the KRT7 expression was absent in the other AdPCa cell lines (LNCaP, C4-2B, and VCaP) and NEPCa cell line H660. The expression of KRT7 mRNA generally correlated well with its protein expression, except for the NEPCa cell line H660.

The KRT7 population in HuPSA exhibited low to negligible expression of androgen receptor (AR) and AR signaling activity (Fig. 4B). Also, this population expressed low to no prostate lineage and differentiation markers FOXA1, HOXB13, and NKX3-1 (sFig. 1 & Fig. 4), suggesting that the cells in this population have switched lineage away from luminal epithelia (Fig. 4B).

Further, we identified the signaling pathways enriched in the KRT7 population. We found that the Wnt signaling pathway, an important stem signaling that controls cell fate determination and cell proliferation[2], was active in this population. Additionally, several transcription factors, including TCF4, PAX6, NFE2L2, and HNF4G, were identified as upstream regulators of this population (sFig. 8).

Krt7 population in MoPSA

For the Krt7 population in MoPSA, GEM samples were the major cell source, contributing 80% (32,011 of 39,891) of the cells in this population. This population expressed low to no basal markers Krt5, Krt14 and Trp63, like their counterpart in HuPSA (sFig. 1). However, unlike the KRT7 population in HuPSA, the MoPSA Krt7 population expressed Ar and exhibited high levels of Ar signaling activity (Fig. 4B). Additionally, the murine Krt7 population expressed moderate levels of Hoxb13 and Foxa1 (sFig. 1), suggesting that the murine Krt7 population still sustains the prostatic luminal epithelial lineage.

In addition to GEM, wild type prostate samples contributed to the Krt7 population as well (sFig. 2). Previous studies have shown that Krt7 is expressed in prostate basal epithelial cells. However, our analysis indicates that the Krt7 population in MoPSA are non-basal. To investigate the possible biological function of Krt7 population in murine prostate, we analyzed the "GSE146811" dataset generated by Sawyers' group, which was also included in MoPSA. This dataset contains prostate samples collected from mice at various time points during androgen-mediated prostate regeneration [29]. Our analysis focused on the GSE146811-derived non-basal epithelial cells defined by MoPSA. These cells' scRNAseq data were visualized on the UMAP (Fig. 5M) and the sample source was color coded and labelled in Fig. 5N. These figures depicted a clear prostate regeneration path from intact, castration (CX) to regeneration (R). While majority of the cells were in the LE/AdPCa_1, a normal population of MoPSA, it is interesting to note that some cells (mostly derived from the prostate of CX 14-day wild type mice) were in the AdPCa_2, a cancer population (Fig. 5M), suggesting the high similarity (e.g., low Pbsn expression) in their transcriptomes to this type of prostate cancer cells.

The cells of Krt7 population were mostly derived from CX 28-day samples and some CX 14-day samples (Figs. 5M and 5N). sFig. 7 provided a split view of the same plot, it clearly illustrated the position of each sample during prostate regeneration.

To validate the Krt7 populational changes during prostate regeneration, we conducted immunostaining to assess the Krt7 expression in prostate tissues. As depicted in Figs. 5O-T, in the prostate tissues derived from intact mice, Krt7 expression was absent in the majority of luminal epithelial cells but was present in some rare luminal epithelia that were located at the tips of the gland. However, following castration from 7 days to 21 days, the proportion of Krt7+ luminal cells gradually

increased. After testosterone supplement for 1 day to 15 days, the proportion of Krt7+ luminal epithelial cells gradually decreased, reverting to baseline level like those in intact prostate. This suggests that the positive expression of Krt7 may label the prostatic luminal epithelial cells that have survived androgen deprivation. This was further corroborated by the Krt7 expression pattern in the TRAMP tumors. In the prostatic intraepithelial neoplasia (PIN) tumors developed intact TRAMP mice, Krt7 was only expressed in a small subset of PIN cells and majority PIN cells did not express this gene (Fig. 5U). However, Krt7 was extensively expressed in the PIN lesions in castrated TRAMP mice (Fig. 5V). Similar to those castrate-resistant cells in wild type prostate, the Krt7 positive PIN cells in castrated TRAMP are likely the cells that have survived androgen deprivation. TRAMP mice develop NEPCa after castration[30]. It is interesting to note that Krt7 was expressed in the residual PIN cells but not in NEPCa cells (Fig. 5V).

MMP7 labels the club population

HuPSA also revealed a cell population, Club, that was clustered together with basal cells and highly expressed MMP7 gene (Fig. 1). This population was recently discovered in a scRNAseq study, which is also included in our HuPSA data. It was defined as "club" cells based on the expression of marker genes of the club cells in lung, including PIGR, MMP7, and CP[28,31]. The Club population was present in HuPSA but not in MoPSA. This population were characterized by the high expression of MMP7 and WFDC2 (sFig. 1). MMP7 encodes the smallest secreted matrix metalloproteinase[32]. WFDC2 encodes a protease inhibitor[33]. The MMP7 population displayed low CNV (sFig. 6), therefore are likely non-cancer cells. As depicted in Fig. 6C, MMP7 was expressed in the Club population, whereas WFDC2 was expressed in both Club and Basal populations. This expression pattern was also observed in the immunostaining analysis. As shown in Fig. 6D, MMP7 expression was detected in a subset of luminal epithelial cells in human benign prostatic hyperplasia (BPH) samples. On the serial section, WFDC2 expression was detected in the basal layer as well as the areas positive for MMP7 immunostaining. Moreover, dual immunofluorescence staining results showed that MMP7 was co-expressed with luminal marker KRT8 but not basal marker KRT5 (Fig. 6E), indicating that the Club population, although clustered together with basal cells, are luminal epithelial cells.

4. Progenitor-like cells in HuPSA and MoPSA

The Progenitor-like cluster was only present in HuPSA. It was predominantly contributed by mCRPCa samples (sFig. 2). In line with this, the cells in this cluster harbored high CNVs (sFig. 6). The Progenitor-like cluster was located in between the Luminal and NEPCa clusters on UMAP plot (Fig. 1). The cells in this cluster highly expressed SOX2 and FOXA2, two genes that are expressed in both embryonic prostate and NEPCa (sFig. 1). However, the majority of the progenitor-like cells expressed low or no NEPCa markers such as NCAM1 and INSM1 (sFig. 1). This population expressed low to no AR and AR targets (KLK3 and NKX3-1), indicating a low AR signaling in these cells. Additionally, these cells expressed low to no FOXA1 or HOXB13, two prostatic lineage markers (sFig.1), suggesting a poorly differentiated state of these cells.

The Progenitor-like cluster was absent in MoPSA. However, a Pou2f3 cluster, unique to MoPSA, displayed certain progenitor features. This cluster was characterized by the expression of Pou2f3, a marker of the cells that are in a transition state from AdPCa to NEPCa[26]. The Pou2f3 cells were also identified in pTen:Rb:p53 double/triple knock-out mouse models[7]. These cells expressed Sox2 (Fig. 6A), thus they might be the murine counterpart of progenitor-like cells in HuPSA.

5. Human NEPCa Can Be Further Detailed into Subpopulations, Unlike Mouse NEPCa

The transcriptomes of NEPCa cells were extracted from HuPSA and MoPSA datasets and visualized on UMAP for higher resolution. The results indicate that the human NEPCa cells could be further divided into different sub-populations, whereas the mouse NEPCa population was relatively uniform. Through unsupervised clustering and examination of marker genes, the HuPSA NEPCa cells were classified into five sub-populations: CHGA, NEUROD1, G2M, TOX, and STAT3 (Fig. 3A). All NEPCa sub-populations exhibited high expression levels of NE markers INSM1 and NCAM1 (CD56) (sFigs. 5A-C).

The CHGA subpopulation expressed high levels of the NE marker CHGA (Fig. 3D). It represents the canonical NE phenotype in PCa. The other NEPCa sub-populations expressed relatively low but non-negligible levels of CHGA.

The expression of ASCL1, a driver transcription factor of NEPCa[34], was detected in all the NEPCa subpopulations except NEUROD1. The NEUROD1+ sub-population was characterized by the high expression of NEUROD1. It exhibited high Wnt signaling activity (Fig. 3B). This is consistent with a previous study which has demonstrated that Wnt signaling activates NEUROD1 expression during neurogenesis in mice[35]. By examining the feature plots of NEUROD1 and ASCL1 in HuPSA, we discovered an exclusive expression pattern between NEUROD1 and ASCL1 (Fig. 3D).

The G2M sub-population was characterized by the high expression of the signature genes of cell cycle G2M phase such as NUCKS1, TOP2A, CENPF (sTable 5). In contrast, the other subpopulations exhibited evenly distribution of the S and G2M phases (sFig. 5D). The fact that G2M subpopulation stands out as a group suggests these cells may have prolonged G2M phase and higher level of DNA damage compared with the other subpopulations.

The TOX sub-population was characterized by the high expression of Thymocyte selection-associated HMG box gene (TOX). These cells exhibited elevated activity in the VEGF signaling pathway and high expression of TCF4, a transcription factor of Wnt signaling (Figs. 3B-D).

The STAT3 sub-population not only expressed high levels of the STAT3 gene but also displayed high activity in JAK-STAT signaling and the transactivation of STAT3 target genes, suggesting this sub-population might be driven by JAK-STAT3 signaling (Figs. 3B-D).

6. Non-epithelial clusters

In addition to epithelial clusters, the HuPSA and MoPSA visualized stromal, endothelial, and immune cells as well. The Stromal cluster can be further separated into three populations, Fibroblast, Smooth muscle, and Pericyte, for both species. A large population of T cells were detected in HuPSA (Fig. 1). Based on the Sankey diagrams (sFig. 2), these T cells were mainly contributed by normal adjacent and AdPCa samples. The other histology groups (normal, benign, cribriform, CSPC, CRPCa and mCRPCa samples) contained fewer T cells. This is consistent with the clinical observation that advanced PCa is an immunologically “cold” tumor.

7. HuPSA-based deconvolution of RNAseq data re-classified human PCa specimens and identified novel KRT7 and progenitor-like samples

Bulk RNA-seq is commonly used in PCa research to identify diagnostic markers and potential treatment targets. However, bulk RNA-seq data can only reflect the averaged gene expression in a mixed

cell population. Also, PCa is heterogenous and intratumor heterogeneity complicates molecular classification of tumors. The gene expression profiles established in HuPSA for each cell population can be used to overcome these challenges. The HuPSA dataset integrated RNAseq data of 368,831 cells at single cells resolution and spanned various types of cell populations. Each population was defined based on its transcriptome profile. By employing covariance-based deconvolution technology against bulk RNA-seq data [36], we can estimate the populational composition for each PCa sample and define its molecular subtype.

In this study, we analyzed publicly available bulk RNAseq data that were derived from 877 prostatic specimens. We examined each sample's composition of the following populations: Luminal, KRT7, Basal, Club, Progenitor-like, NEPCa, Stromal (Fibroblast, SM, Pericyte), and Immune. The luminal populations were combined into a single group because of the relatively small differences in their transcriptomes. The prostatic tissues were re-classified based on their dominant populational composition. As shown in Fig. 7, most specimens can be re-classified as Luminal (n=570), KRT7 (n=9), Progenitor-like (n=7), and NEPCa (n=43). Samples contained more than one dominant cell populations were assigned to three mixture groups: KRT7/AdPCa mix (n=1), progenitor-like/AdPCa mix (n=1), and NEPCa/AdPCa mix (n=1). Samples with a low percentage of dominant population were categorized as unclassified (n=167). The contaminated samples (n=78) were dominant with stromal or immune cells, containing few cancer cells.

The Luminal group consisted samples from both Normal prostate (n=67) and AdPCa tumors based on their original histology record. Among the AdPCa tumors, 293 samples expressed AR mRNA at high levels (>30) and the other 210 samples expressed low levels of AR.

To facilitate data transparency and for researchers to visualize the expression of their genes of interest in prostatic cells on HuPSA , similar to our previous CTPC App[37], we generated a web App (https://pcatools.shinyapps.io/ProAtlas_dev/) to visualize the gene expression in human samples. Researchers can visualize the mRNA expression level of their genes of interest in these newly defined cell populations including the rare KRT7 and progenitor-like cells.

8. HuPSA projection of C42B xenograft scRNAseq data revealed treatment-induced neuroendocrine differentiation population

Using the HuPSA as a road map, we analyzed our own scRNASeq data derived from C4-2B xenograft that were under androgen deprivation and Enzalutamide treatments. A HuPSA-based dimension reduction and label transfer were performed against the C4-2B data. This allowed us to successfully identify human cancer populations and mouse stromal populations. Interestingly, similar to the AdPCa sub-populations in HuPSA, the cells in C4-2B derived xenograft could also be classified into AdPCa_AR+_1, AdPCa_AR+_2, AdPCa_AR lo, and AdPCa_proliferating populations. Moreover, the C42B-derived NEPCa population was also identified (Fig. 8B). Furthermore, we visualized the expression of AR and KLK3 genes in the C42B xenograft cancer populations. The AdPCa_AR+ cells expressed AR and maintained high KLK3 expression. The AdPCa_AR- cells expressed low levels of AR but still exhibited high KLK3 expression. In contrast, the NEPCa cells did not express AR or KLK3 but showed high levels of the NE marker gene INSM1 (Figs. 8C & 8D). These findings suggest that PCa cells may employ diverse mechanisms to acquire treatment resistance. Additionally, the expression of the cell cycle marker gene TOP2A supported the proliferative nature of the AdPCa_proliferating and NEPCa cells.

Discussion

Advanced technologies have revolutionized our ability to understand biological questions. RNA sequencing, for instance, provides unbiased and high-throughput gene expression profiling data. Furthermore, single cell RNA sequencing technology enables researchers to investigate transcriptome at single-cell resolution and address old questions in cancer research in new ways, such as the tumor microenvironment and immune response, as well as newly proposed challenges like phenotypic plasticity, cellular senescence, and non-mutational epigenetic reprogramming[47]. HuPSA and MoPSA, as integrated scRNAseq datasets, have the capability to detect various cell populations and visualize cancer cells of different phenotypes on dimensional reduction maps. By analyzing differentially expressed genes, upstream transcription factor activities, and signaling pathway activities, both atlases can provide insights into the driver mechanisms of phenotypic plasticity and shed light on potential druggable targets for different phenotypes.

HuPSA and MoPSA can serve as immune landscapes for different PCa subtypes by providing counts of different immune cells within specific samples or groups of samples. Furthermore, the characterization of immune populations using existing bulk RNA-seq data has been an area of interest for several years. Our pipeline, which utilizes HuPSA to deconvolute PCa patient bulk RNA-seq data, can be repurposed to decipher the immune composition within PCa tissue.

HuPSA and MoPSA also hold great potential for uncovering cancer-stromal interactions. Cellular communication often relies on ligand-receptor interactions. By utilizing the existing ligand-receptor database "CellChatDB," we predicted ligand-receptor pairs between and within the populations in HuPSA and MoPSA. As depicted in sFig. 8, the complex network of cell-cell interactions highlights the necessity to expand our research scope beyond cancer cells and delve into the entire tumor microenvironment. Genes that are not expressed in cancer cells may still contribute to tumor growth, and signaling pathways activated in cancer cells may not have direct effects on the cancer cells themselves.

While integrated scRNAseq datasets like HuPSA and MoPSA provide valuable insight for studying epigenetic reprogramming, cell lineage and cancer progression, these large-scale data still have limitations. For example, scRNAseq, at transcriptome level, cannot effectively differentiate early-stage cancer (AdPCa_AR+) from the normal luminal epithelial cells. It is possible that the data integration process minimized the differences between these populations. However, differential expression analysis on luminal epithelial cells (cells from normal tissues) and early-stage AdPCa cells using non-integrated data could not well differentiate these two populations either. This indicates that even in the untransformed raw transcriptome, there is only minimal difference between these populations. Therefore, scRNAseq may not be the optimal tool for characterizing the early stages of carcinogenesis, which are primarily driven by DNA alterations.

Another drawback pertains to the analysis of scRNAseq data itself. The high-throughput nature of scRNAseq data, with its complex multi-dimensional gene expression profiles, can be overwhelming for human interpretation. Transcriptome identities are defined by thousands of gene expression values along numerous axes in a multi-dimensional space. To aid visualization, dimensional reduction techniques such as PCA, t-SNE, and UMAP are applied to reduce the data to lower dimensions. However, it is important for researchers to recognize that the transcriptome identities represented on UMAP plots are not a perfect reflection of reality. In addition, the visual representation can change significantly based on the choice of dimensional reduction parameters. In our opinion, as a famous ancient Chinese

poet Su Shi eloquently put it, "It's a range viewed in face and peaks viewed from the side, assuming different shapes viewed from far and wide.", researchers should objectively process the scRNAseq data using appropriate pipelines, but data interpretation may still be subjective.

Methods

1. Single-cell RNA sequencing on TRAMP and C42B xenograft tumors

Human and mouse prostate tumor tissues were harvested and dissociated using “Tumor Dissociation Kit, human, #130-095-929” and “Tumor Dissociation Kit, mouse, #130-096-730” from Miltenyi Biotec. The dead cells were removed by “Dead Cell Removal Kit, #130-090-101” from Miltenyi Biotec. The red blood cells were removed by “Red Blood Cell Lysis Solution, # 130-094-183” from Miltenyi Biotec. Then the cDNA libraries were constructed using Chromium Next GEM Single Cell 3’ Reagent Kit v3.1. cDNA was fragmented, processed, and size selected. Adaptors were ligated and samples were cleaned up. Dual indexes were attached via PCR. The completed libraries were cleaned up and assessed for quality with the Agilent TapeStation D5000 High Sensitivity Kit. Libraries were quantitated with qPCR (NEBNext Library Quant Kit for Illumina, Bio-rad CFX96 Touch Real-Time PCR). Libraries were normalized to 1.5 pM and pooled. The library pool was denatured and diluted to approximately 300 pM. A library of 1.5 pM PhiX was spiked in as an internal control. Paired-end sequencing was performed on an Illumina NovaSeq 6000.

3. scRNAseq Data integration and processing

Single-cell read count data were load into R environment using “loadFry” function from Fishpond package[50]. Subsequently “Seurat V5”[51] was used for quality control, data integration, UMAP dimensional reduction, clustering, annotation and C42B data projection. Quality control was performed based on the total RNA count and feature count for each cell. Cells with extremely low or high RNA/feature counts were excluded to ensure the removal of low-quality and doublets. The RPCA model was used for data integration. In the integration process, each study (instead of sample) was treated as one "batch" to prevent over integration. After the UMAP dimensional reduction and clustering, the clusters were then labeled with assign population names based on the marker genes expression and original histology information. The human lung V2 (HLCA) annotated reference dataset from “Azimuth”[52] were referred manually for immune and stromal populations annotation. The R package “SCpubr”[53] was used for data visualization. Dim plots were utilized to visualize the populations of HuPSA and MoPSA on UMAP. Feature plots were employed to visualize gene expression on the UMAP. Geyser plots were used to visualize and quantify gene expression. Sankey plots were used to depict the "flow" of cells between populations, histology, and study groups. The single cell copy number alterations were calculated and visualized using “InferCNV” package[54]. Pathway activity was calculated by “decoupleR”[55]. Transcription factor activity was calculated using “dorothea”[55]. The “CSCDRNA” package[36] was used for HuPSA based bulk RNAseq deconvolution. The “CellChat” package[56] was used to predict ligand-receptor pairs in HuPSA and MoPSA. All detailed parameters were described in the R scripts deposited to GitHub pages.

4. Bulk RNAseq data collection and processing

The human PCa bulk RNAseq data raw FASTQ files was collected from multiple cohorts. GEO accessions: GSE120795[57], GSE126078[58], GSE156289[59], GSE114740, GSE217260, GSE179321[60], GSE112786[61], GSE104131[62], GSE31528[63], GSE54460[64], GSE22260[65], GSE216490[66]; dbGaP accessions:

phs000909.v1.p1[42], phs000915.v2.p2[3]. The TCGA_PRAD read counts and TPM data were acquired using "recount3"[67] R package. The sequencing reads were aligned to human GRCh38 genome (from NCBI) using STAR[68] and Salmon[69]. The nf-core/rnaseq pipeline was used for software environment, paralleling and quantity control. Linux ubuntu was used as the operating system. Samples were considered high quality and retained if they met the following criteria: duplicated reads less than 60%, total reads more than 20 million, and STAR unique mapped percentage higher than 70%. However, the TCGA samples were not filtered as these specific metrics were not available. Eventually 877 high quality samples from normal, BPH, tumor, primary, AdPCa, CRPCa, mCRPCa, NEPCa, organoid, PDX (patient-derived xenograft) histology groups were kept and used for further HuPSA based deconvolution.

5. PCa cell line xenografts

Archived tissues of PCa cell line derived xenografts were used in IHC staining. C4-2B cells (1 million cells per graft) were mixed with Matrigel and subcutaneously injected into SCID mice. When the tumors reach 100 mm3, the tumor bearing mice were castrated. One week post castration, the mice were treated with Enzalutamide (10 mg/kg body weight, ip) 3 times a week for 3 weeks. At the end of experiment, the mice were sacrificed, and tumors were excised for analysis.

6. Mouse castration and Testosterone treatments

Wild-type mice were obtained from Jackson laboratory (Bar Hrbor, ME). Mice at 8 weeks of age were used for this study. Mice were divided into 3 groups: intact group, surgically castrated group and surgically castrated mice given exogenous testosterone replacement at 3 weeks post-castration. Additionally, the castrated mice group were divided into two subgroups based on the time since surgery, consisting of 7 days and 21 days. Meanwhile, the castrated mice receiving exogenous testosterone replacement were further divided into six groups based on the duration of testosterone treatment, which included 1 day, 2days, 3 days, 4 days, 7 days, and 15 days. All isolated prostate tissue was fixed in 10% neutral buffered formalin for embedding and sectioning. All animal procedures were performed in accordance with institutional guidelines and approved by the Animal care and Use committee at the LSU Health Shreveport.

7. Immunohistochemical, immunofluorescence staining and Western blot

De-identified human prostate tissue specimens were obtained from LSU Health-Shreveport Biorepository Core, Overton Brooks VA Medical Center, Ochsner Health System Biorepository and Tissue for Research as described previously[70].

Immunostaining was performed using Vectastain elite ABC peroxidase kit (Vector Laboratories, Burlingame, CA). Primary antibodies include KRT7 (abclonal, A4357), MMP7 (abclonal, A0695), CK5 (BioLegend, 904801), CK8 (BioLegend,904801). The tissue sections were counterstained, mounted, and imaged with a Zeiss microscope (White Plains, NY). Cells were collected in PBS and lysed in passive lysis buffer (Promega, Madison, WI).

Equal amounts of protein were loaded for Western blot analyses. ProSignal Dura ECL Reagent (Genesee Scientific, San Diego, CA) and Chemidoc (Bio-Rad, Hercules, CA) were used to visualize the proteins. Beta-tubulin was used as loading control.

Acknowledgement:

We thank the Broad Institute for generating high-quality sequence data supported by NHGRI funds (grant # U54 HG003067) with Eric Lander as PI. We also thank Stand Up To Cancer-Prostate Cancer Foundation Prostate Dream Team Translational Cancer Research Grant for supporting generated high-quality data used in this manuscript. The datasets used in this manuscript were obtained from dbGaP at http://www.ncbi.nlm.nih.gov/gap through dbGaP accession number phs000909 and phs000915. We also thank Weill Cornell Medical College for the samples collection.

References

1 Society, A. C. *Key Statistics for Prostate Cancer*, <https://www.cancer.org/cancer/prostate-cancer/about/key-statistics.html> (2022).

2 Yeh, Y. *et al.* Wnt/Beta-catenin signaling and prostate cancer therapy resistance. *Prostate Cancer*, 351-378 (2019).

3 Robinson, D. *et al.* Integrative clinical genomics of advanced prostate cancer. *Cell* **161**, 1215-1228 (2015).

4 Cheng, S. *et al.* Neuroendocrine prostate cancer has distinctive, non-prostatic HOX code that is represented by the loss of HOXB13 expression. *Scientific reports* **11**, 1-11 (2021).

5 Beltran, H. *et al.* Aggressive variants of castration-resistant prostate cancer. *Clinical Cancer Research* **20**, 2846-2850 (2014).

6 Bluemn, E. G. *et al.* Androgen receptor pathway-independent prostate cancer is sustained through FGF signaling. *Cancer cell* **32**, 474-489 (2017).

7 Chan, J. M. *et al.* Lineage plasticity in prostate cancer depends on JAK/STAT inflammatory signaling. *Science*, eabn0478 (2022).

8 Ferguson, A. M. & Rubin, M. A. Lineage plasticity in prostate cancer: Looking beyond intrinsic alterations. *Cancer letters* **548**, 215901 (2022).

9 Mu, P. *et al.* SOX2 promotes lineage plasticity and antiandrogen resistance in TP53-and RB1-deficient prostate cancer. *Science* **355**, 84-88 (2017).

10 Zhang, X. *et al.* SRRM4 expression and the loss of REST activity may promote the emergence of the neuroendocrine phenotype in castration-resistant prostate cancer. *Clinical Cancer Research* **21**, 4698-4708 (2015).

11 Rotinen, M. *et al.* ONECUT2 is a targetable master regulator of lethal prostate cancer that suppresses the androgen axis. *Nature medicine* **24**, 1887-1898 (2018).

12 Bishop, J. L. *et al.* The master neural transcription factor BRN2 is an androgen receptor–suppressed driver of neuroendocrine differentiation in prostate cancer. *Cancer discovery* **7**, 54-71 (2017).

13 Akamatsu, S. *et al.* The placental gene PEG10 promotes progression of neuroendocrine prostate cancer. *Cell reports* **12**, 922-936 (2015).

14 Dong, B. *et al.* Single-cell analysis supports a luminal-neuroendocrine transdifferentiation in human prostate cancer. *Communications biology* **3**, 778 (2020).

15 Heidegger, I. *et al.* Comprehensive characterization of the prostate tumor microenvironment identifies CXCR4/CXCL12 crosstalk as a novel antiangiogenic therapeutic target in prostate cancer. *Molecular Cancer* **21**, 132 (2022).

16 Hirz, T. *et al.* Dissecting the immune suppressive human prostate tumor microenvironment via integrated single-cell and spatial transcriptomic analyses. *Nature Communications* **14**, 663 (2023).

17 Wong, H. Y. *et al.* Single cell analysis of cribriform prostate cancer reveals cell intrinsic and tumor microenvironmental pathways of aggressive disease. *Nature Communications* **13**, 6036 (2022).
18 Kim, W. K. *et al.* Aberrant androgen action in prostatic progenitor cells induces oncogenesis and tumor development through IGF1 and Wnt axes. *Nature communications* **13**, 1-18 (2022).
19 Terzic, J. *et al.* Hypoxia-inducible factor 1A inhibition overcomes castration resistance of prostate tumors. *EMBO Molecular Medicine*, e17209 (2023).
20 Zhu, Y. *et al.* Targeting the chromatin effector Pygo2 promotes cytotoxic T cell responses and overcomes immunotherapy resistance in prostate cancer. *Science Immunology* **8**, eade4656 (2023).
21 Germanos, A. A. *et al.* Defining cellular population dynamics at single-cell resolution during prostate cancer progression. *Elife* **11**, e79076 (2022).
22 Graham, M. K. *et al.* Single-cell atlas of epithelial and stromal cell heterogeneity by lobe and strain in the mouse prostate. *The Prostate* **83**, 286-303 (2023).
23 Hiroto, A. *et al.* Stromal androgen signaling acts as tumor niches to drive prostatic basal epithelial progenitor-initiated oncogenesis. *Nature Communications* **13**, 6552 (2022).
24 Qiu, X. *et al.* MYC drives aggressive prostate cancer by disrupting transcriptional pause release at androgen receptor targets. *Nature communications* **13**, 2559 (2022).
25 Troiani, M. *et al.* Single-cell transcriptomics identifies Mcl-1 as a target for senolytic therapy in cancer. *Nature communications* **13**, 2177 (2022).
26 Brady, N. J. *et al.* Temporal evolution of cellular heterogeneity during the progression to advanced AR-negative prostate cancer. *Nature Communications* **12**, 3372 (2021).
27 Lee, D.-H. *et al.* Androgen action in cell fate and communication during prostate development at single-cell resolution. *Development* **148**, dev196048 (2021).
28 Song, H. *et al.* Single-cell analysis of human primary prostate cancer reveals the heterogeneity of tumor-associated epithelial cell states. *Nature communications* **13**, 141 (2022).
29 Karthaus, W. R. *et al.* Regenerative potential of prostate luminal cells revealed by single-cell analysis. *Science* **368**, 497-505 (2020).
30 Grabowska, M. M. *et al.* Mouse models of prostate cancer: picking the best model for the question. *Cancer and Metastasis Reviews* **33**, 377-397 (2014).
31 Henry, G. H. *et al.* A cellular anatomy of the normal adult human prostate and prostatic urethra. *Cell reports* **25**, 3530-3542 (2018).
32 Liao, H.-Y., Da, C.-M., Liao, B. & Zhang, H.-H. Roles of matrix metalloproteinase-7 (MMP-7) in cancer. *Clinical biochemistry* **92**, 9-18 (2021).
33 Lamy, P.-J., Plassot, C. & Pujol, J.-L. Serum HE4: an independent prognostic factor in non-small cell lung cancer. *PloS one* **10**, e0128836 (2015).
34 Nouruzi, S. *et al.* ASCL1 activates neuronal stem cell-like lineage programming through remodeling of the chromatin landscape in prostate cancer. *Nature Communications* **13**, 2282 (2022).
35 Kuwabara, T. *et al.* Wnt-mediated activation of NeuroD1 and retro-elements during adult neurogenesis. *Nature neuroscience* **12**, 1097-1105 (2009).
36 Karimnezhad, A. More accurate estimation of cell composition in bulk expression through robust integration of single-cell information. *Bioinformatics Advances* **2**, vbac049 (2022).
37 Cheng, S. & Yu, X. CTPC, a combined transcriptome dataset of prostate cancer cell lines. *bioRxiv* (2022).
38 Zou, M. *et al.* Transdifferentiation as a mechanism of treatment resistance in a mouse model of castration-resistant prostate cancer. *Cancer discovery* **7**, 736-749 (2017).

39 Hansel, D. E. *et al.* Shared TP53 gene mutation in morphologically and phenotypically distinct concurrent primary small cell neuroendocrine carcinoma and adenocarcinoma of the prostate. *The Prostate* **69**, 603-609 (2009).
40 Mertz, K. D. *et al.* Molecular characterization of TMPRSS2-ERG gene fusion in the NCI-H660 prostate cancer cell line: a new perspective for an old model. *Neoplasia* **9**, 200-IN203 (2007).
41 Tomlins, S. A. *et al.* Role of the TMPRSS2-ERG gene fusion in prostate cancer. *Neoplasia* **10**, 177-IN179 (2008).
42 Beltran, H. *et al.* Molecular characterization of neuroendocrine prostate cancer and identification of new drug targets. *Cancer discovery* **1**, 487-495 (2011).
43 Yuan, T.-C., Veeramani, S. & Lin, M.-F. Neuroendocrine-like prostate cancer cells: neuroendocrine transdifferentiation of prostate adenocarcinoma cells. *Endocrine-related cancer* **14**, 531-547 (2007).
44 Wright, M. E., Tsai, M.-J. & Aebersold, R. Androgen receptor represses the neuroendocrine transdifferentiation process in prostate cancer cells. *Molecular endocrinology* **17**, 1726-1737 (2003).
45 Shen, R. *et al.* 2 edn 67-75 (Elsevier).
46 Huss, W. J. *et al.* Origin of androgen-insensitive poorly differentiated tumors in the transgenic adenocarcinoma of mouse prostate model. *Neoplasia* **9**, 938-IN931 (2007).
47 Hanahan, D. Hallmarks of cancer: new dimensions. *Cancer discovery* **12**, 31-46 (2022).
48 Li, D. *et al.* ETV4 mediates dosage-dependent prostate tumor initiation and cooperates with p53 loss to generate prostate cancer. *Science Advances* **9**, eadc9446 (2023).
49 He, D. *et al.* Alevin-fry unlocks rapid, accurate and memory-frugal quantification of single-cell RNA-seq data. *Nature Methods* **19**, 316-322 (2022).
50 Zhu, A., Srivastava, A., Ibrahim, J. G., Patro, R. & Love, M. I. Nonparametric expression analysis using inferential replicate counts. *Nucleic Acids Research* **47**, e105-e105 (2019).
51 Hao, Y. *et al.* Dictionary learning for integrative, multimodal and scalable single-cell analysis. *Nature Biotechnology*, 1-12 (2023).
52 Bakken, T. E. *et al.* Comparative cellular analysis of motor cortex in human, marmoset and mouse. *Nature* **598**, 111-119 (2021).
53 Blanco-Carmona, E. Generating publication ready visualizations for single cell transcriptomics using SCpubr. *bioRxiv*, 2022-2002 (2022).
54 Puram, S. V. *et al.* Single-cell transcriptomic analysis of primary and metastatic tumor ecosystems in head and neck cancer. *Cell* **171**, 1611-1624 (2017).
55 Badia-i-Mompel, P. *et al.* decoupleR: ensemble of computational methods to infer biological activities from omics data. *Bioinformatics Advances* **2**, vbac016 (2022).
56 Jin, S. *et al.* Inference and analysis of cell-cell communication using CellChat. *Nature communications* **12**, 1-20 (2021).
57 Suntsova, M. *et al.* Atlas of RNA sequencing profiles for normal human tissues. *Scientific data* **6**, 36 (2019).
58 Labrecque, M. P. *et al.* Cabozantinib can block growth of neuroendocrine prostate cancer patient-derived xenografts by disrupting tumor vasculature. *Plos one* **16**, e0245602 (2021).
59 Cejas, P. *et al.* Subtype heterogeneity and epigenetic convergence in neuroendocrine prostate cancer. *Nature communications* **12**, 5775 (2021).
60 Luo, G. *et al.* circITGA7 Acts as a miR-370-3p sponge to suppress the proliferation of prostate cancer. *Journal of Oncology* **2021** (2021).
61 Puca, L. *et al.* Patient derived organoids to model rare prostate cancer phenotypes. *Nature communications* **9**, 2404 (2018).

62 Teslow, E. A. *et al.* Exogenous IL-6 induces mRNA splice variant MBD2_v2 to promote stemness in TP53 wild-type, African American PCa cells. *Molecular oncology* **12**, 1138-1152 (2018).
63 Sowalsky, A. G. *et al.* Whole transcriptome sequencing reveals extensive unspliced mRNA in metastatic castration-resistant prostate cancer. *Molecular Cancer Research* **13**, 98-106 (2015).
64 Long, Q. *et al.* Global transcriptome analysis of formalin-fixed prostate cancer specimens identifies biomarkers of disease recurrence. *Cancer research* **74**, 3228-3237 (2014).
65 Kannan, K. *et al.* Recurrent chimeric RNAs enriched in human prostate cancer identified by deep sequencing. *Proceedings of the National Academy of Sciences* **108**, 9172-9177 (2011).
66 Acosta-Vega, N. L. *et al.* Metabolic pathways enriched according to ERG status are associated with biochemical recurrence in Hispanic/Latino patients with prostate cancer. *Cancer Medicine* **12**, 4306-4320 (2023).
67 Wilks, C. *et al.* recount3: summaries and queries for large-scale RNA-seq expression and splicing. *Genome biology* **22**, 1-40 (2021).
68 Dobin, A. *et al.* STAR: ultrafast universal RNA-seq aligner. *Bioinformatics* **29**, 15-21 (2013).
69 Patro, R., Duggal, G., Love, M. I., Irizarry, R. A. & Kingsford, C. Salmon provides fast and bias-aware quantification of transcript expression. *Nature methods* **14**, 417-419 (2017).
70 Cheng, S. *et al.* The expression of YAP1 is increased in high-grade prostatic adenocarcinoma but is reduced in neuroendocrine prostate cancer. *Prostate cancer and prostatic diseases* **23**, 661-669 (2020).

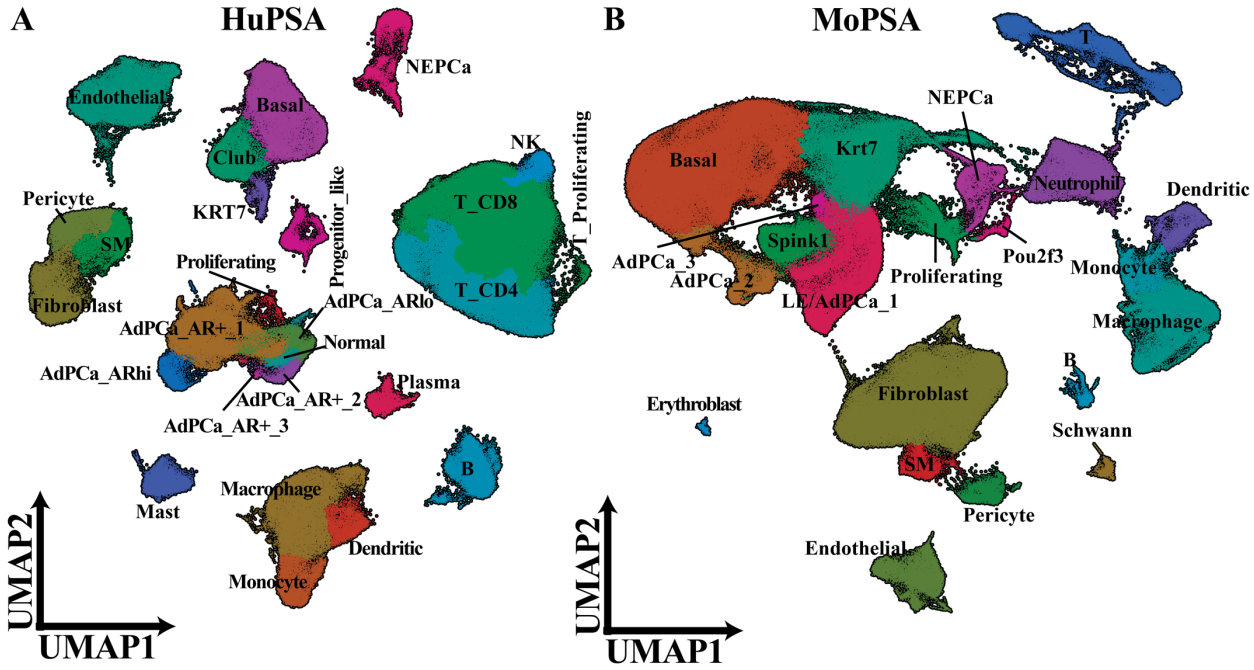

Fig.1: UMAP dimensional reduction of HuPSA (A) and MoPSA (B). Defined cell populations are represented by different colors and text.

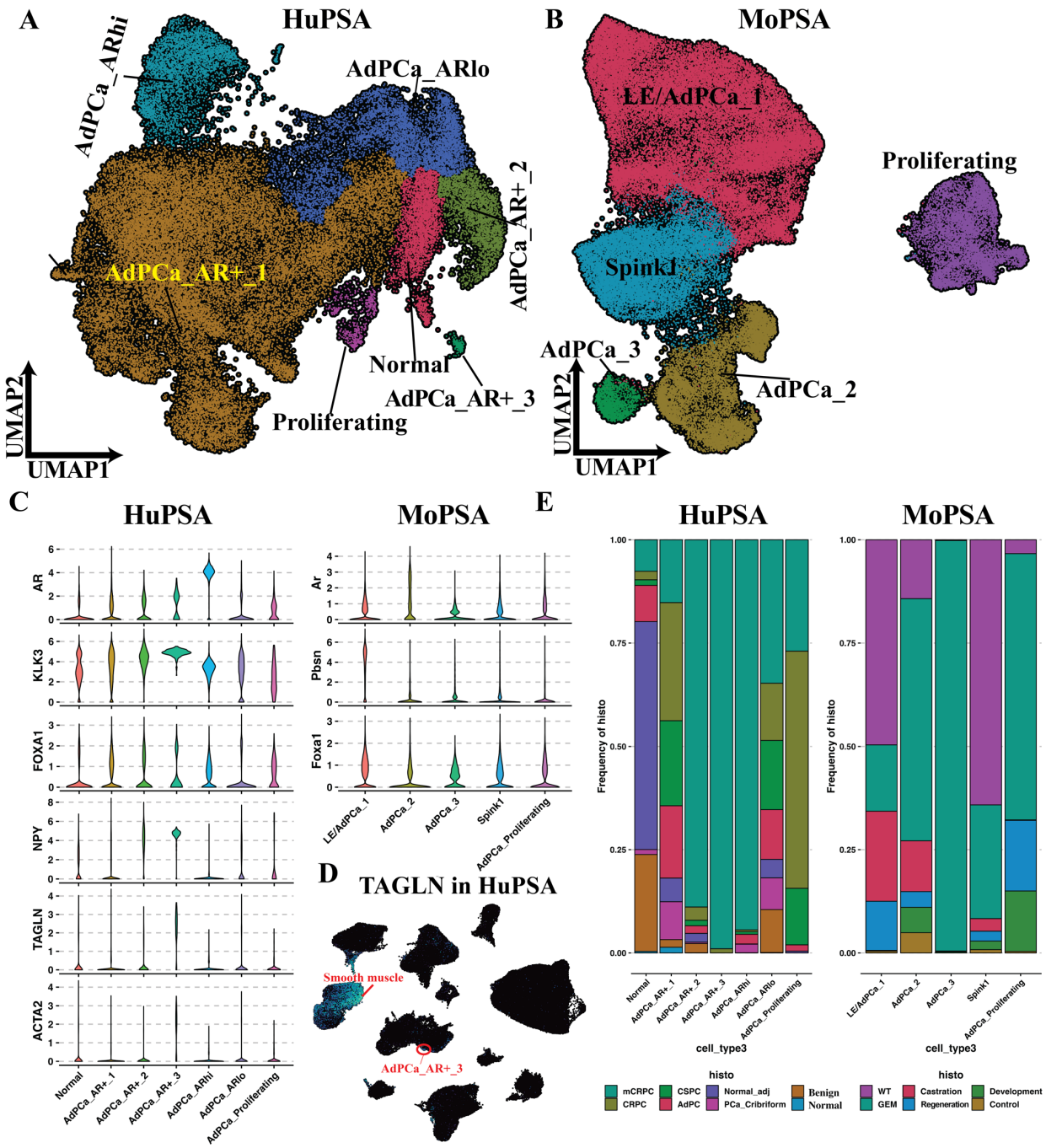

Fig.2: Characterization of AdPCa populations. UMAP dimensional reduction of AdPCa cells from HuPSA (A) and MoPSA (B). Different cell populations within the AdPCa datasets are represented by distinct colors and text labels. Violin plots were utilized to quantify gene expression in different AdPCa subclusters in HuPSA (left) and MoPSA (right). A Feature plot was employed to visualize the expression of the human TAGLN gene specifically in HuPSA. Cells with high expression of TAGLN, namely smooth muscle and AdPCa_AR+_3, are highlighted by text (D). Bar plots were used to depict the composition of histology groups within the different AdPCa subclusters in HuPSA (left) and MoPSA (right).

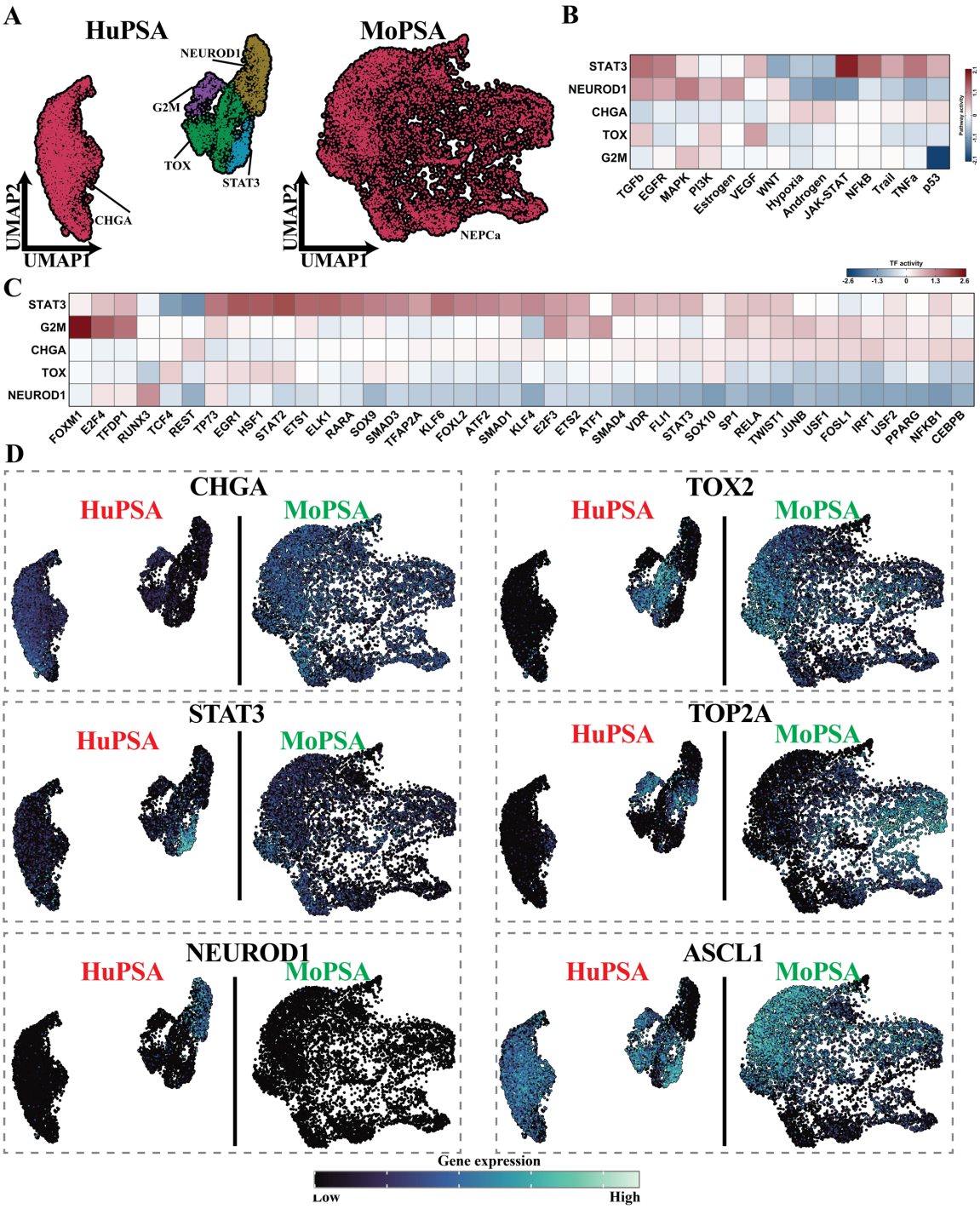

Fig.3: Characterization of NEPCa populations. The UMAP plots revealed heterogenous NEPCa cells in HuPSA and homogenous NEPCa cells in MoPSA, indicating distinct cell population characteristics. Further analysis incorporating clustering and marker gene expression allowed for the subdivision of HuPSA NEPCa cells into 5 subpopulations (A). Heatmaps were employed to illustrate the predicted activity of signaling pathways (B) and upstream transcription factors (C) for the HuPSA NEPCa subclusters, providing insights into their regulatory networks. Additionally, Feature plots were used to visualize the expression of NEPCa subcluster marker genes in both HuPSA and MoPSA datasets (D).

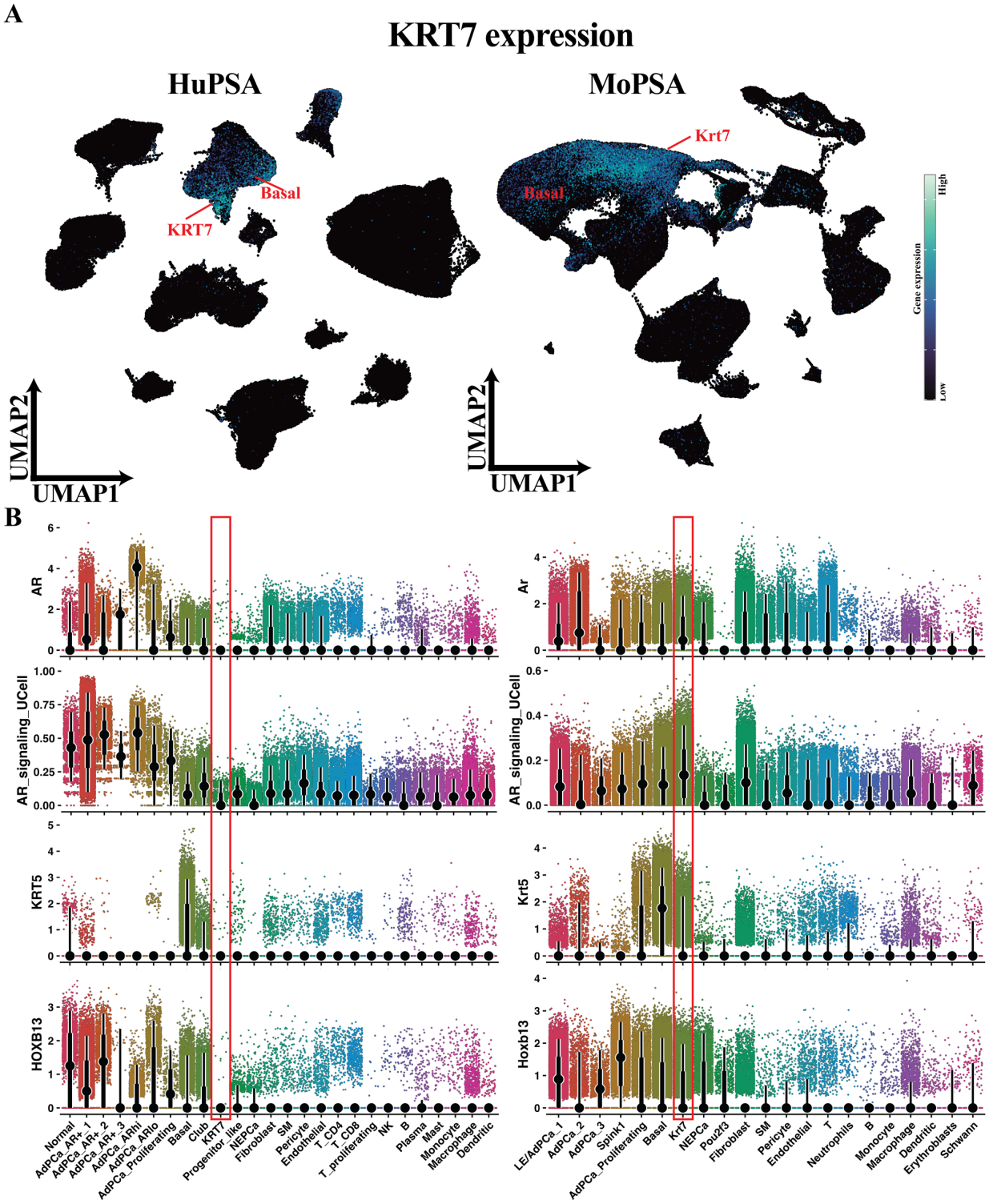

Fig.4: KRT7 gene expression represents unique populations in HuPSA and MoPSA. Feature plots of KRT7 (Krt7 as mouse gene symbol) gene expression showed the KRT7 expressed in KRT7 cluster in HuPSA (left) and Krt7 cluster in MoPSA (right) and some basal epithelium cells in both datasets (A). Geyser plots (scatter plots) quantified genes expression in HuPSA (left) and MoPSA (right). The KRT7/ Krt7 populations were highlighted by red rectangle.

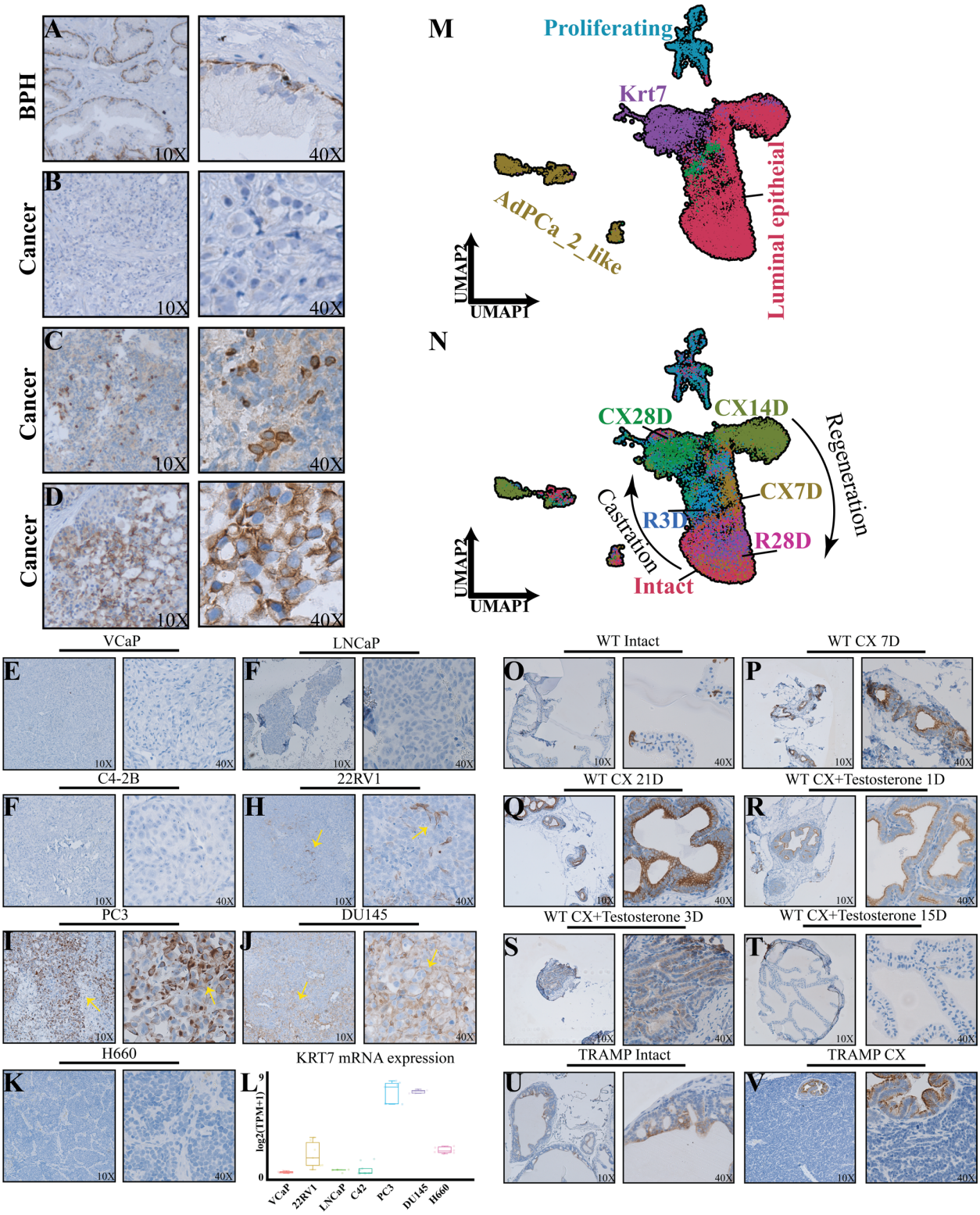

Fig.5: Characterizing KRT7 populations in human and mouse. In human benign prostatic hyperplasia (BPH) tissue, Krt7 was highly expressed in basal epithelium cells but not in luminal epithelium cells (A). Prostate cancer cells showed negative Krt7 expression (B). In some cases, scattered populations (C) or

major populations (D) exhibited high Krt7 expression. Advanced prostate cancer cell line xenograft tissues showed detectable Krt7 expression, with high expression in subpopulations of 22RV1 and PC3 cells, and moderate expression in the majority of DU145 cells (E-K). KRT7 mRNA expression in cultured cells correlated roughly with the IHC staining, with high levels in PC3 and DU145 cells, and low levels in 22RV1 and H660 cells (F). The non-basal epithelial cell populations from “GSE210358” study were isolated from MoPSA and visualized by UMAP as a dim plot (M). The same UMAP plot was labeled with treatment information consisting of intact, castration in 1-28 days and regeneration in 1-14days (N). In wild-type (WT) mouse prostate, Krt7 expression was detected in sub populations both basal and luminal epithelium cells. The normal Krt7+ luminal epithelium cells exhibited resistance to castration (CX). Over the treatment time scale, in intact mouse prostate, Krt7 expression was rarely detected in luminal epithelium cells. However, Krt7+ populations were enriched in CX 7 days and CX 21 days samples. After testosterone treatment, along with luminal epithelium regeneration, the percentage of Krt7+ cells decreased. In transgenic adenocarcinoma of the mouse prostate (TRAMP) tissues, intact mouse tissue showed Krt7 expression in a subpopulation of prostatic intraepithelial neoplasia (PIN) cells. After castration, Krt7 was detected in all PIN cells but not in neuroendocrine prostate cancer cells (O-V).

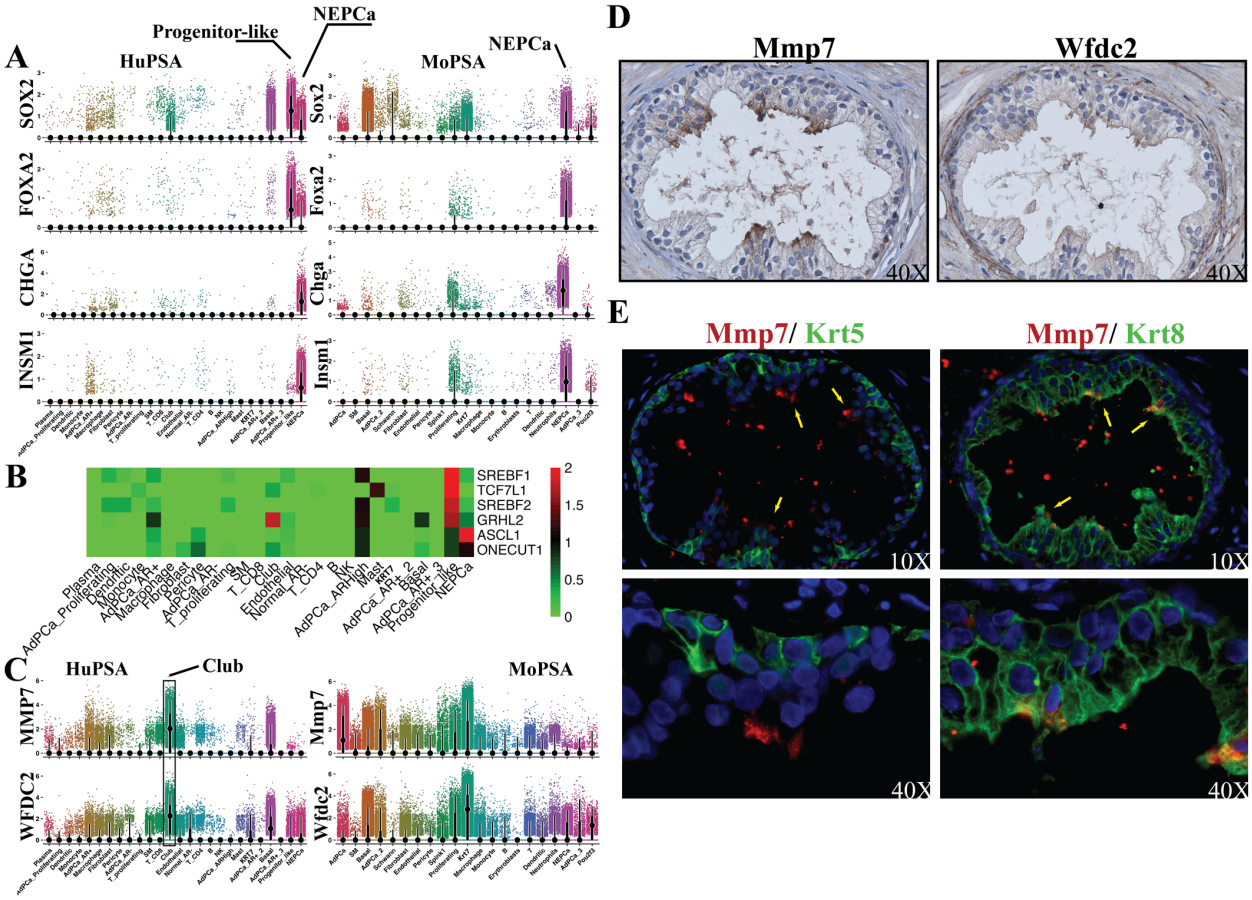

Fig.6: Characterization of HuPSA unique novel populations: Geyser plots depict the expression of progenitor and neuroendocrine marker genes in HuPSA and MoPSA datasets (A). A heatmap reveals predicted upstream regulators associated with progenitor-like and NEPCa populations (B). Geyser plots demonstrate MMP7 and WFDC2 expression in HuPSA and MoPSA (C). Immunohistochemistry on serial sections confirms the presence of Mmp7 and Wfdc2 in specific subpopulations of luminal epithelium cells in human BPH samples (D), while immunofluorescence staining supports the colocalization of Mmp7 with luminal epithelium markers (E).

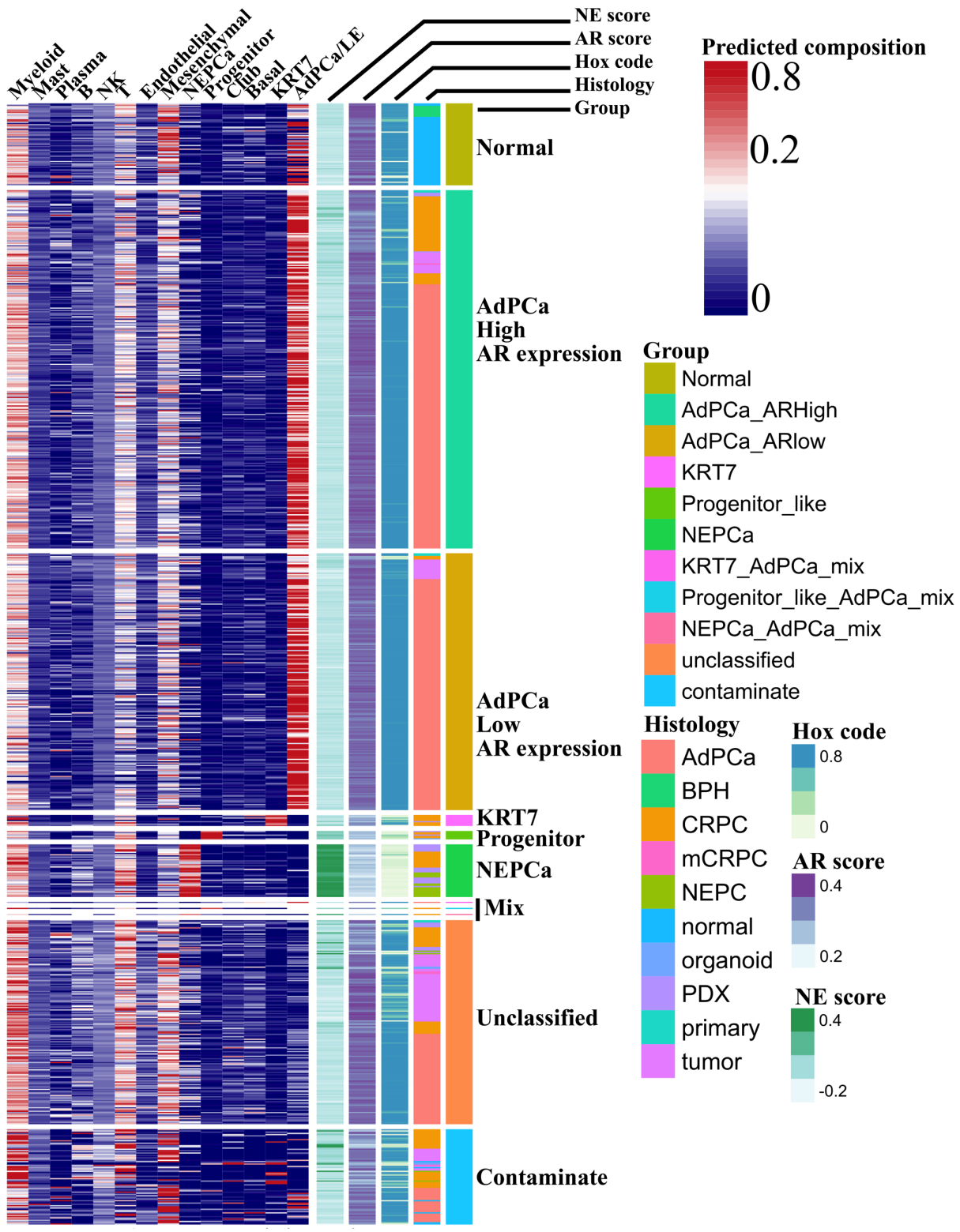

Fig.7: Heatmap of HuPSA-based human PCa bulk RNAseq deconvolution results. Each column in the heatmap represents a cell population defined by HuPSA, while each row corresponds to a bulk RNA sequencing sample. The color in the heatmap indicates the estimated percentage of each cell population within each sample. Additionally, the samples are annotated with NE score, AR score, (prostatic) HOX

code, histology information, and classified group. The samples are categorized into different groups based on the deconvolution results and labeled accordingly. The 'Mix' group contains samples with multiple dominant cancer populations. The 'Unclassified' group comprises samples that did not meet all the criteria for the other groups. The 'Contaminate' group includes samples with a dominant presence of stromal or immune populations.

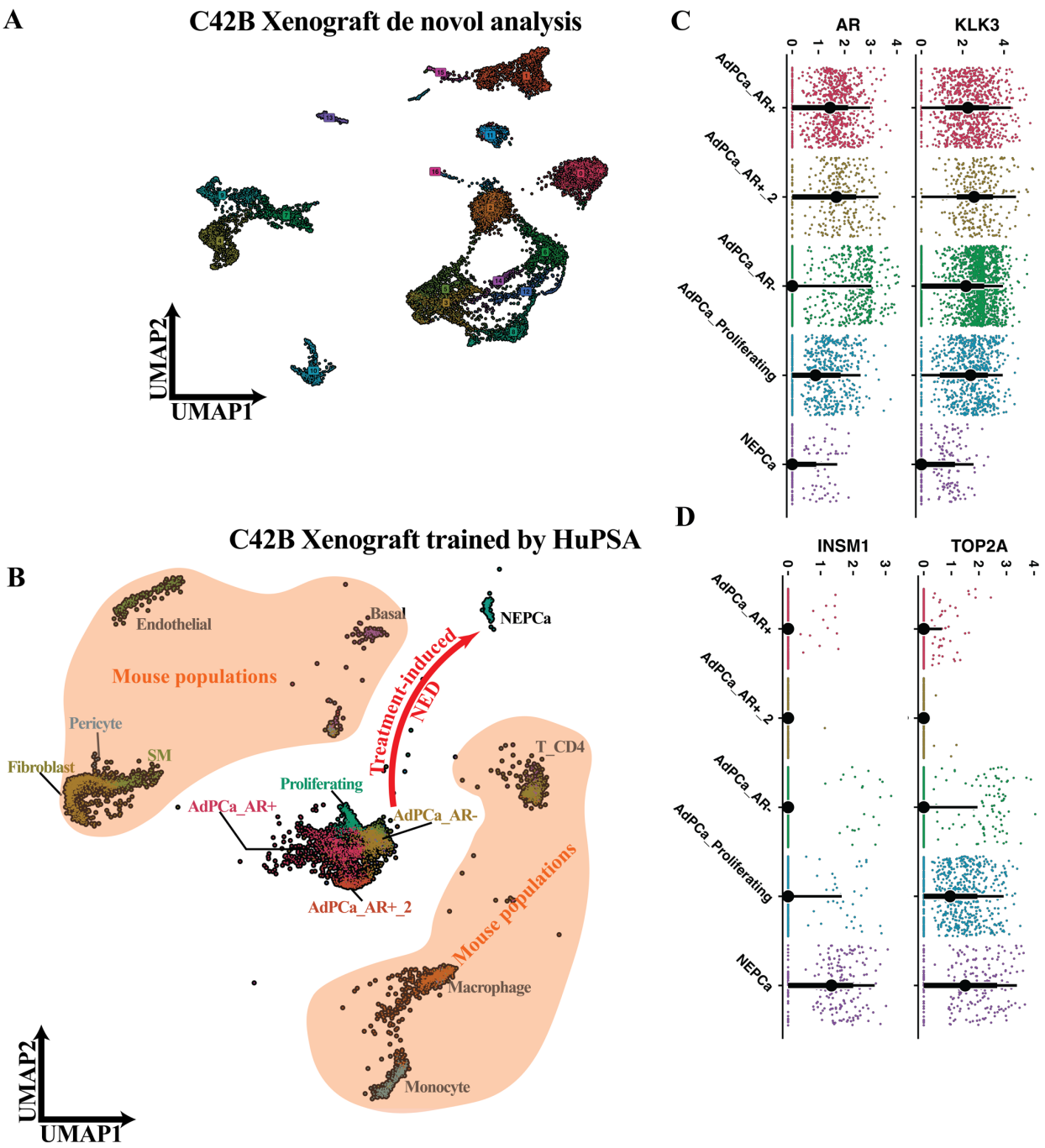

Fig.8: UMAPs of C42B orthotopic xenograft tumor scRNA-seq data. The scRNA-seq data of C42B orthotopic xenograft tumors underwent processing and subsequent UMAP dimensional reduction and clustering (A). Additionally, the same data was subjected to label transfer and supervised projecting using HuPSA, enabling the projection of HuPSA labels onto the C42B scRNA-seq data and facilitating recognizing difference cell populations(B).

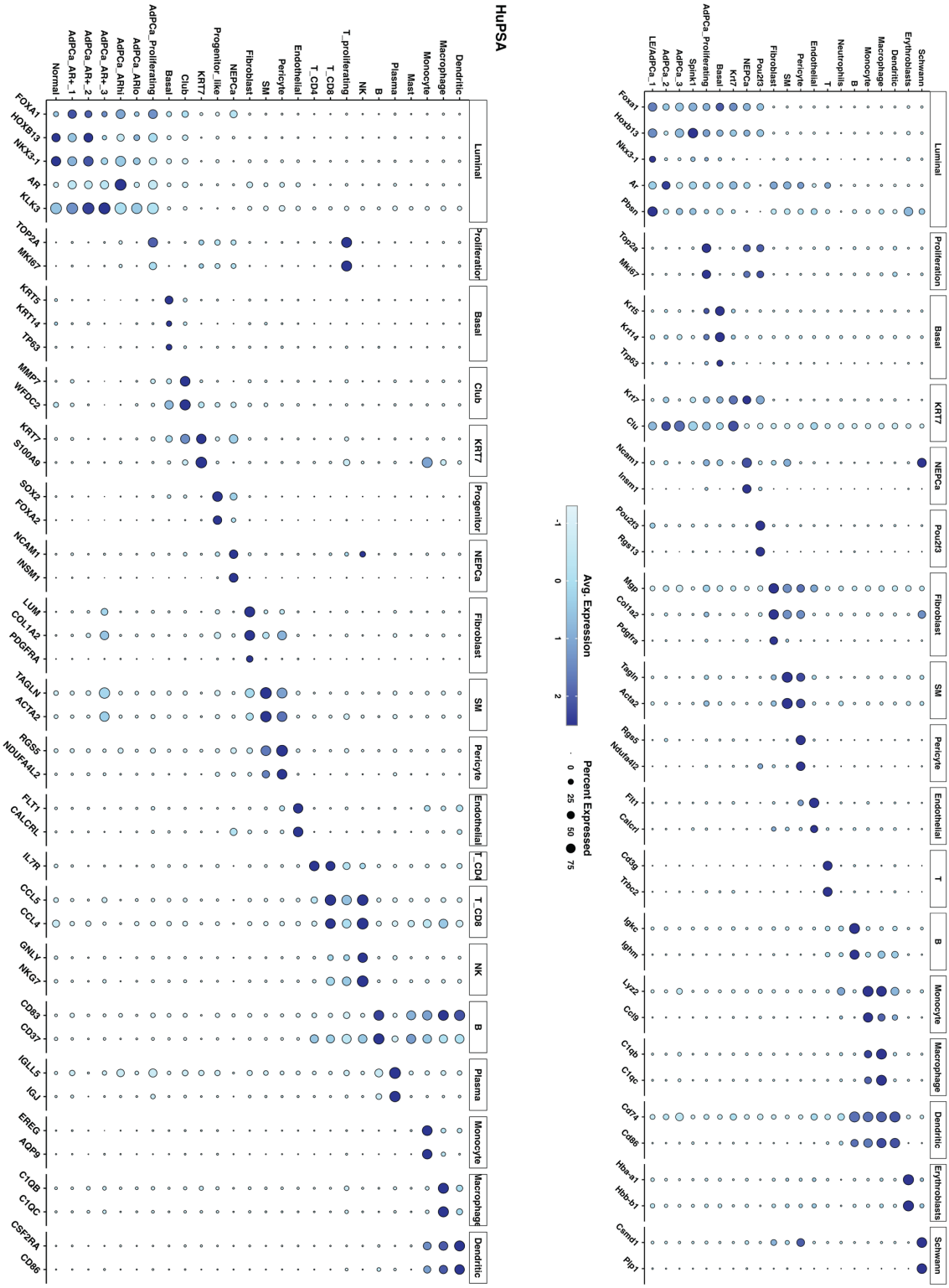

sFig.1: Dot plots visualizing marker gene expression in different populations in HuPSA (left) and MoPSA (right). Each dot represents a gene, and its color represents the gene expression level, ranging from low (light blue) to high (dark blue). The size of the dot corresponds to the percentage of cells expressing that gene within each population.

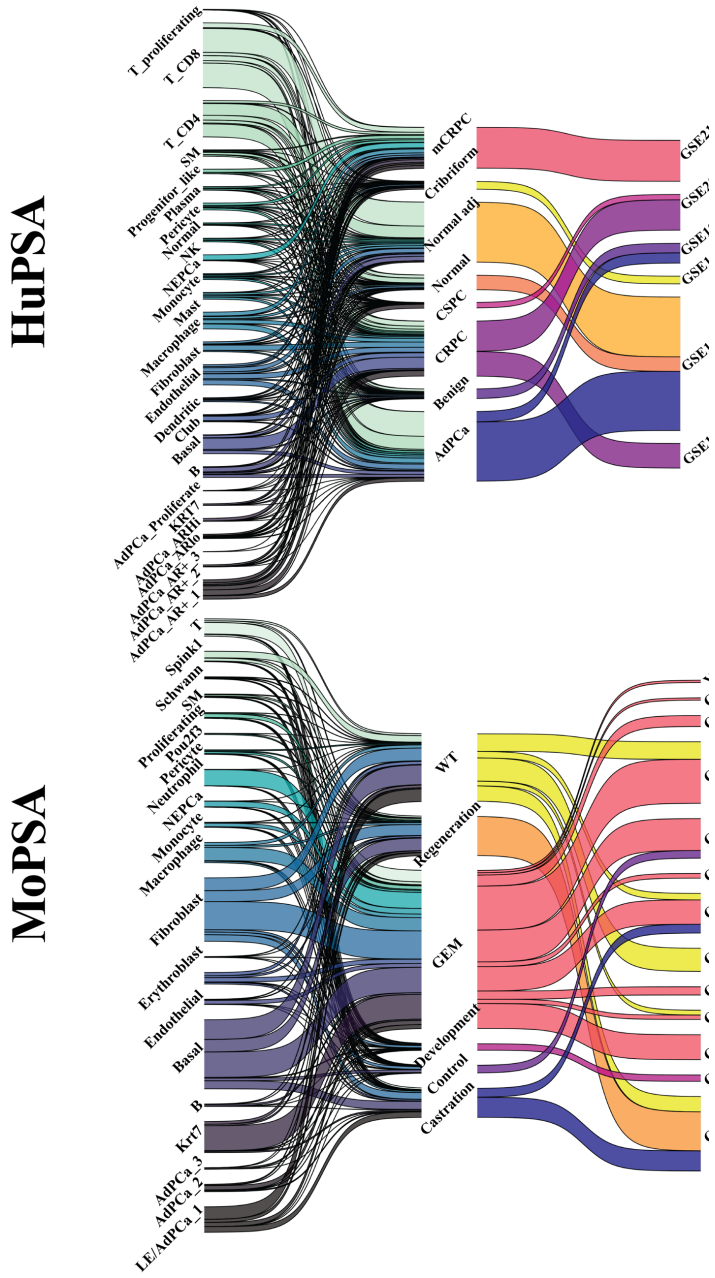

sFig.2: Sankey plots of HuPSA (A) and MoPSA (B) depicting defined cell populations (left), histology groups (middle), and studies (right).

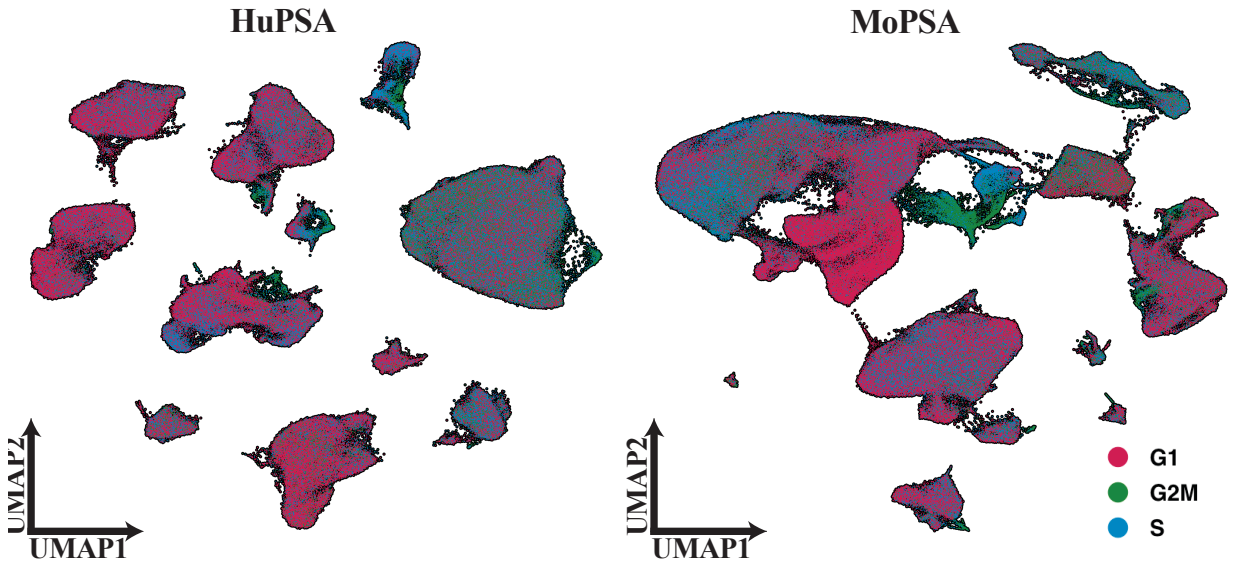

sFig.3: UMAP of HuPSA and MoPSA showing predicted cell phases. G1 phase in red, G2M phase in green, and S phase in blue.

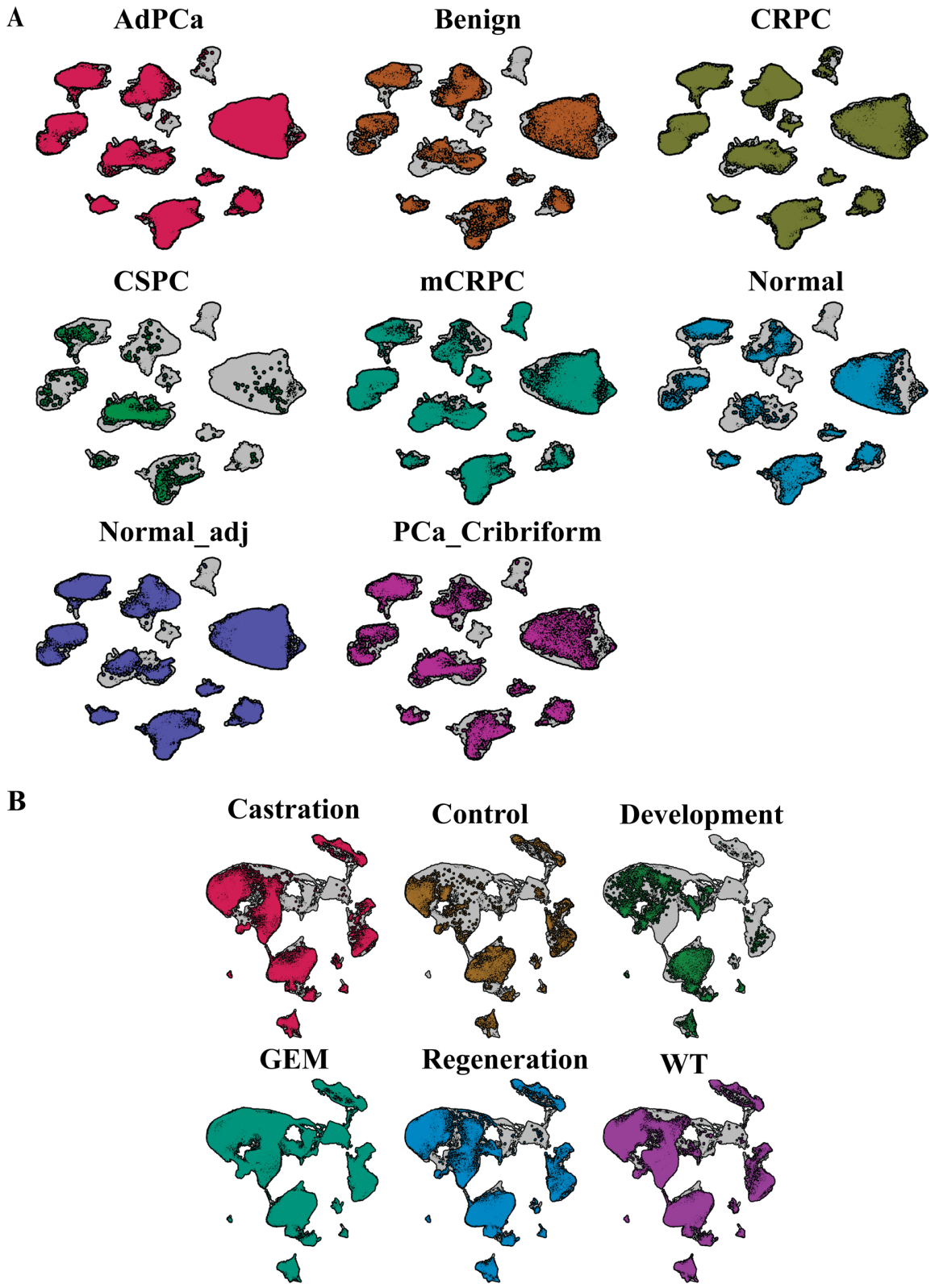

sFig.4: UMAP of HuPSA (A) and MoPSA (B) spited by histology information. Color represents different histology groups defined by original publications.

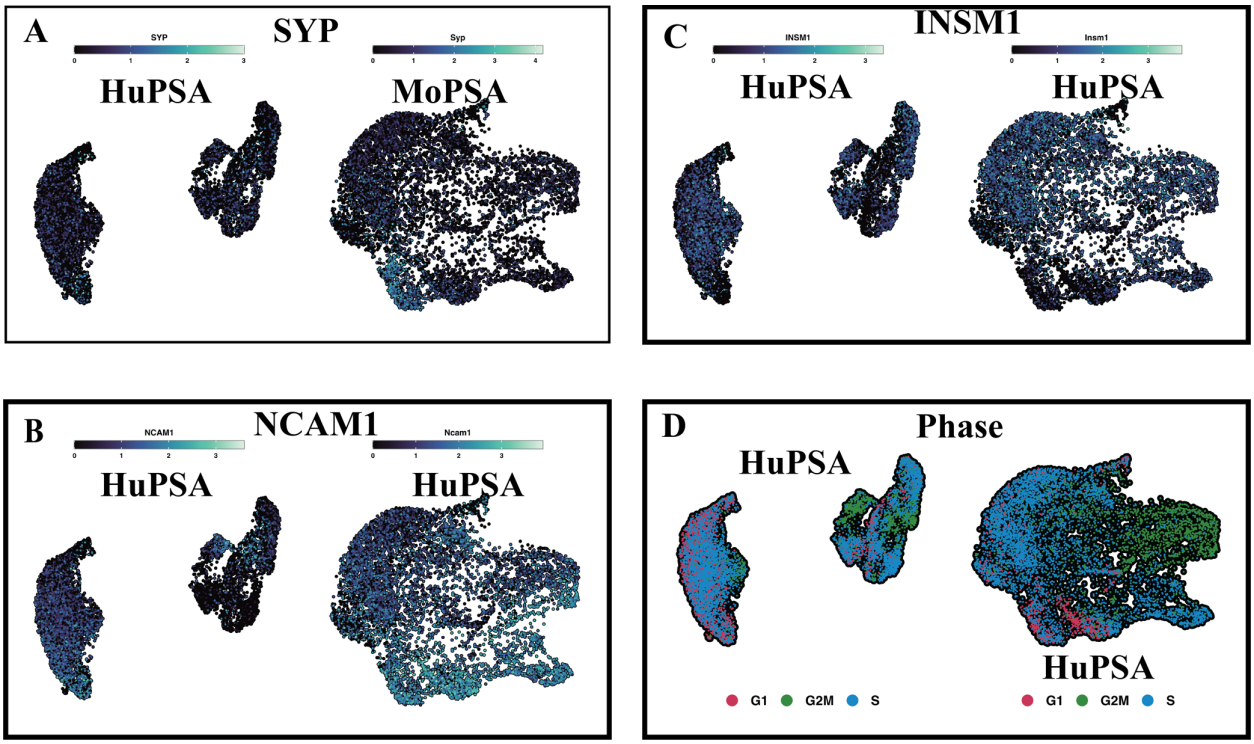

sFig.5: The HuPSA NEPCa sub-populations expressed NE marker genes. The expression of NE marker genes SYP (A), NCAM1 (B) and INSM1 (C) from HuPSA and MoPSa NEPCa cells were visualized by feature plots. The predicted cell cycle phase of NEPCa cells were visualized by Dim plots (D).

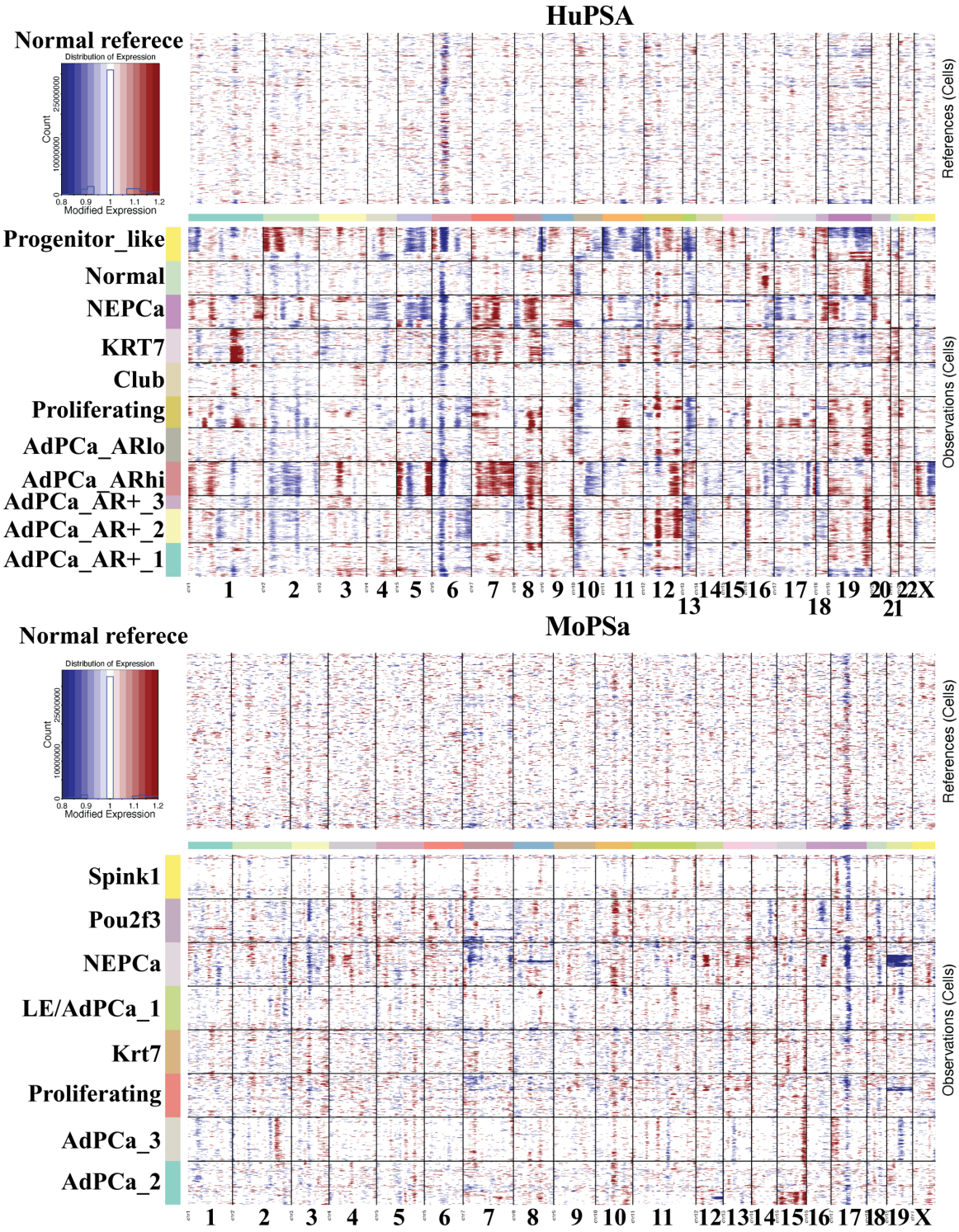

sFig.6: InferCNV results for both HuPSA (up) and MoPSA (down). Heatmaps showed the predicted copy number alterations of selected cell populations compared to normal references (immune and other stromal cell populations).

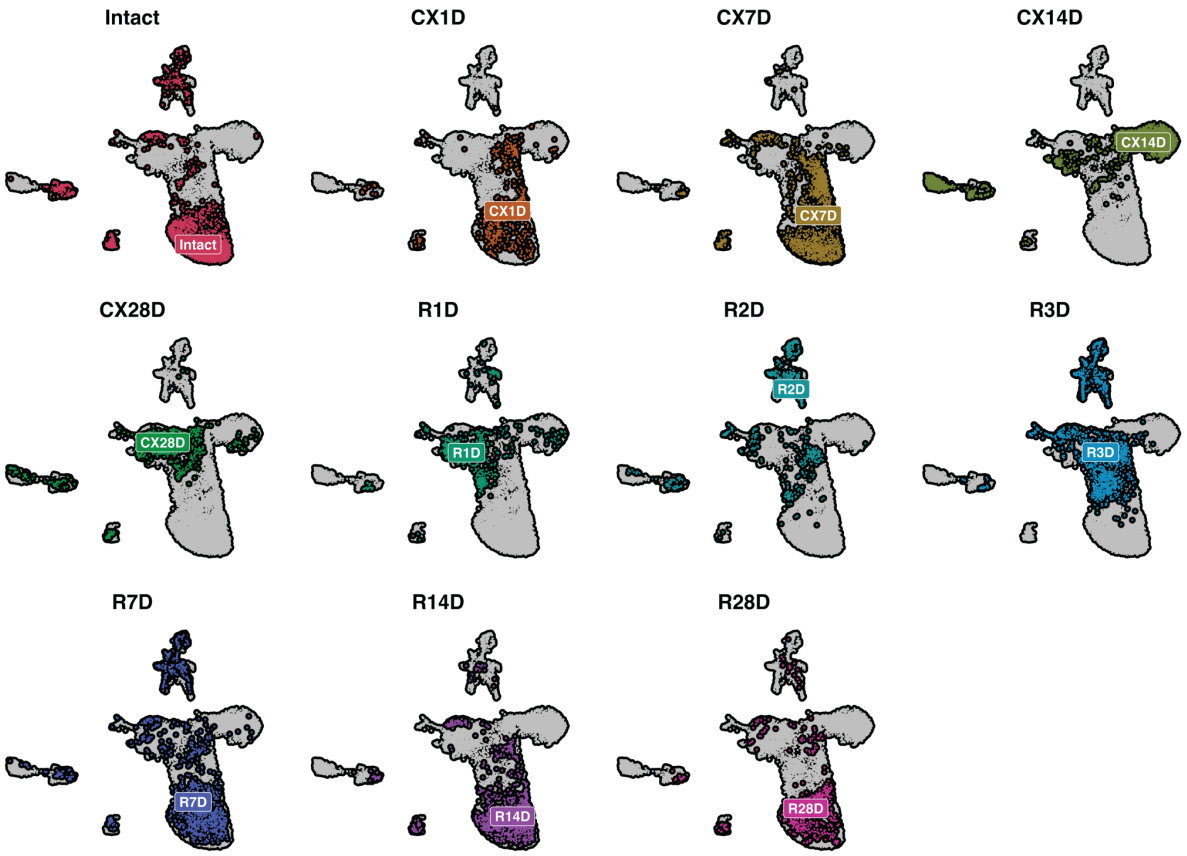

sFig.7: Dim plot of the MoPSA AdPCa and Krt7 populations from castration and regeneration study "GSE146811" labeled by treatment information. This is the split view or Figure5N.

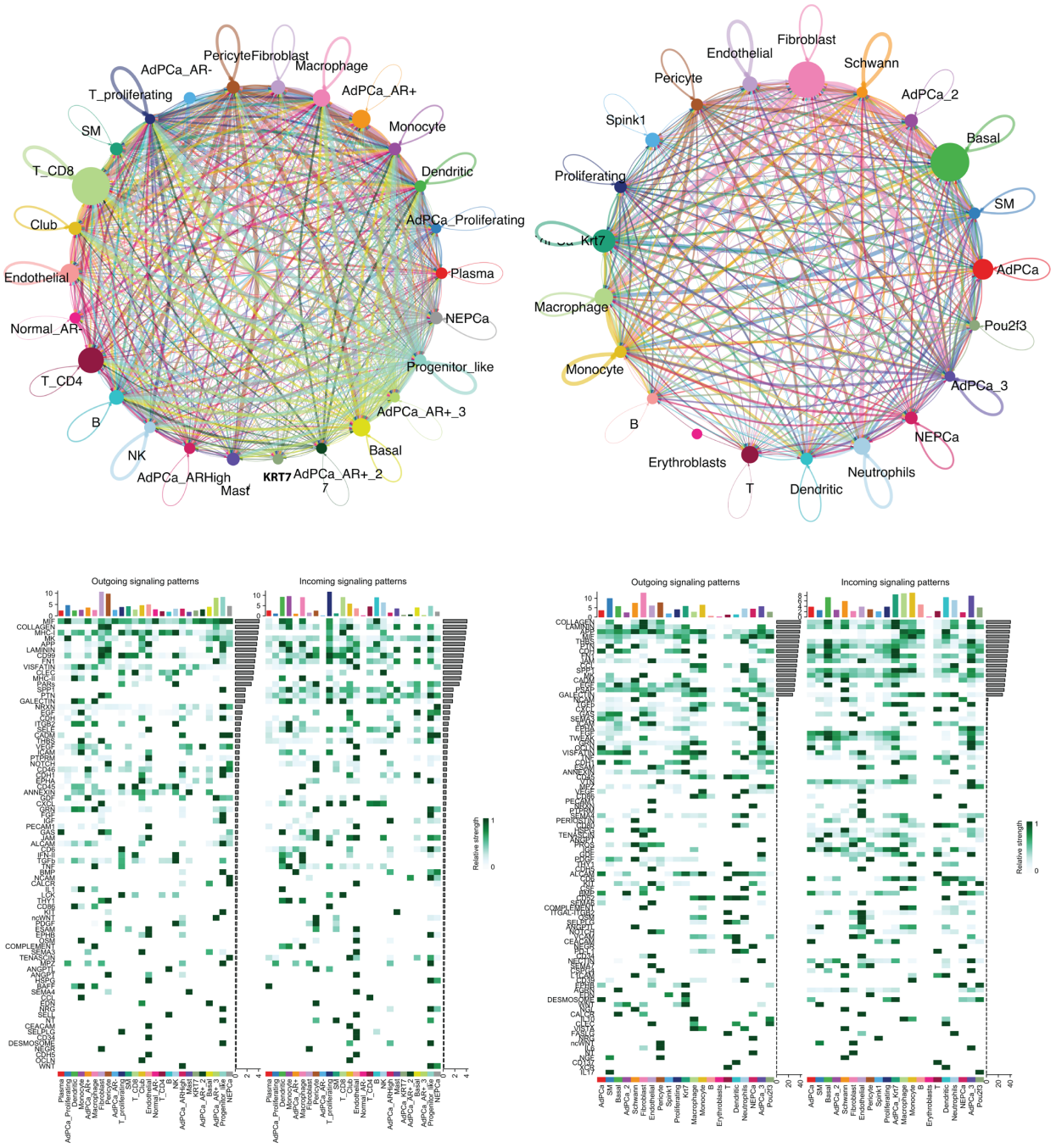

sFig.8: Ligand-receptor analysis on HuPSA and MoPSA. Aggregated cell-cell communication networks were visualized by circle plots for both HuPSA (A) and MoPSA (B). The significant outgoing and incoming signalings were visualized by heatmap for HuPSA (A) and MoPSA (B).

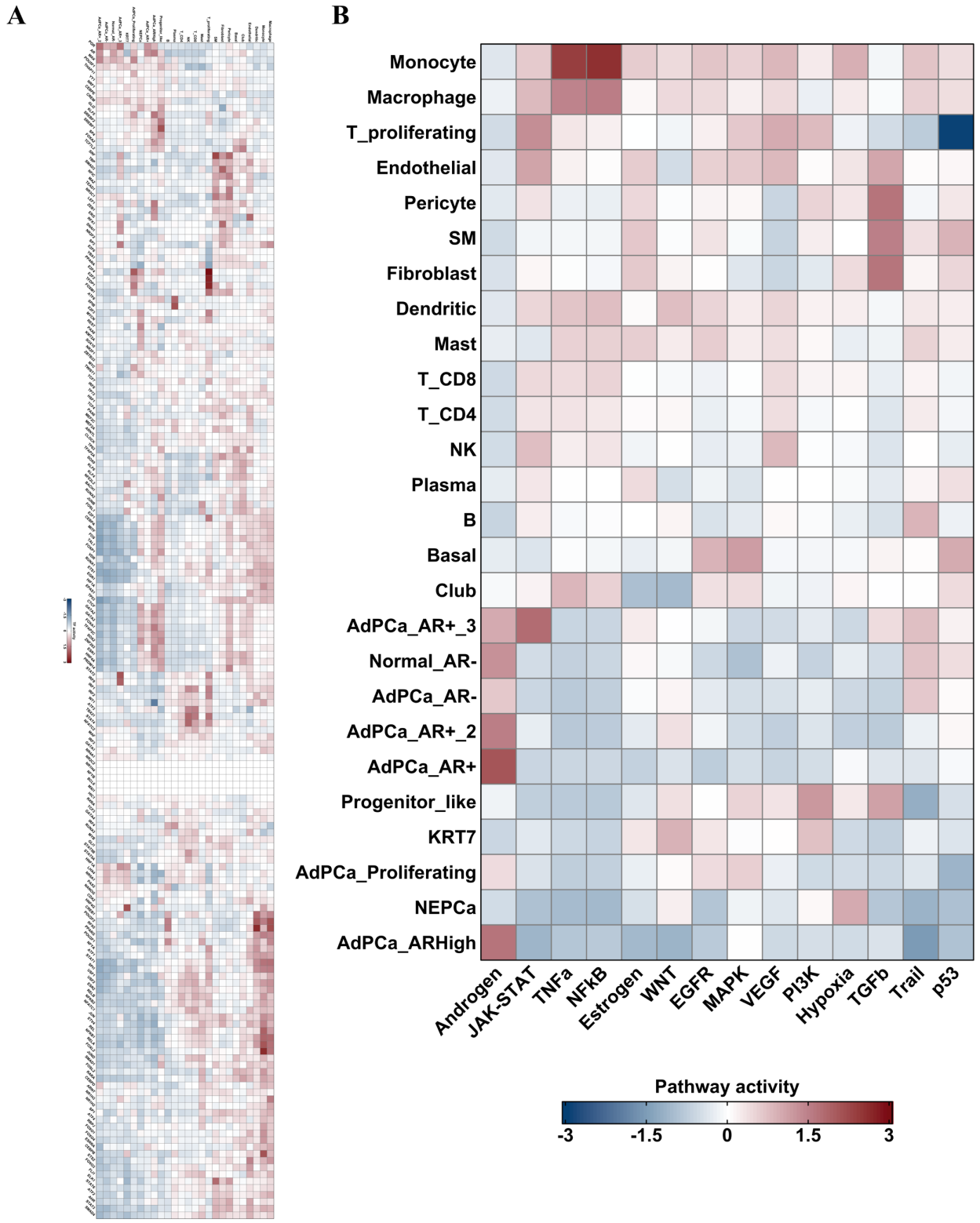

sFig.9: Upstream analysis for HuPSA. Heatmaps were used to visualize the calculated upstream transcription factor activity (A) and signaling pathway analysis for HuPSA.

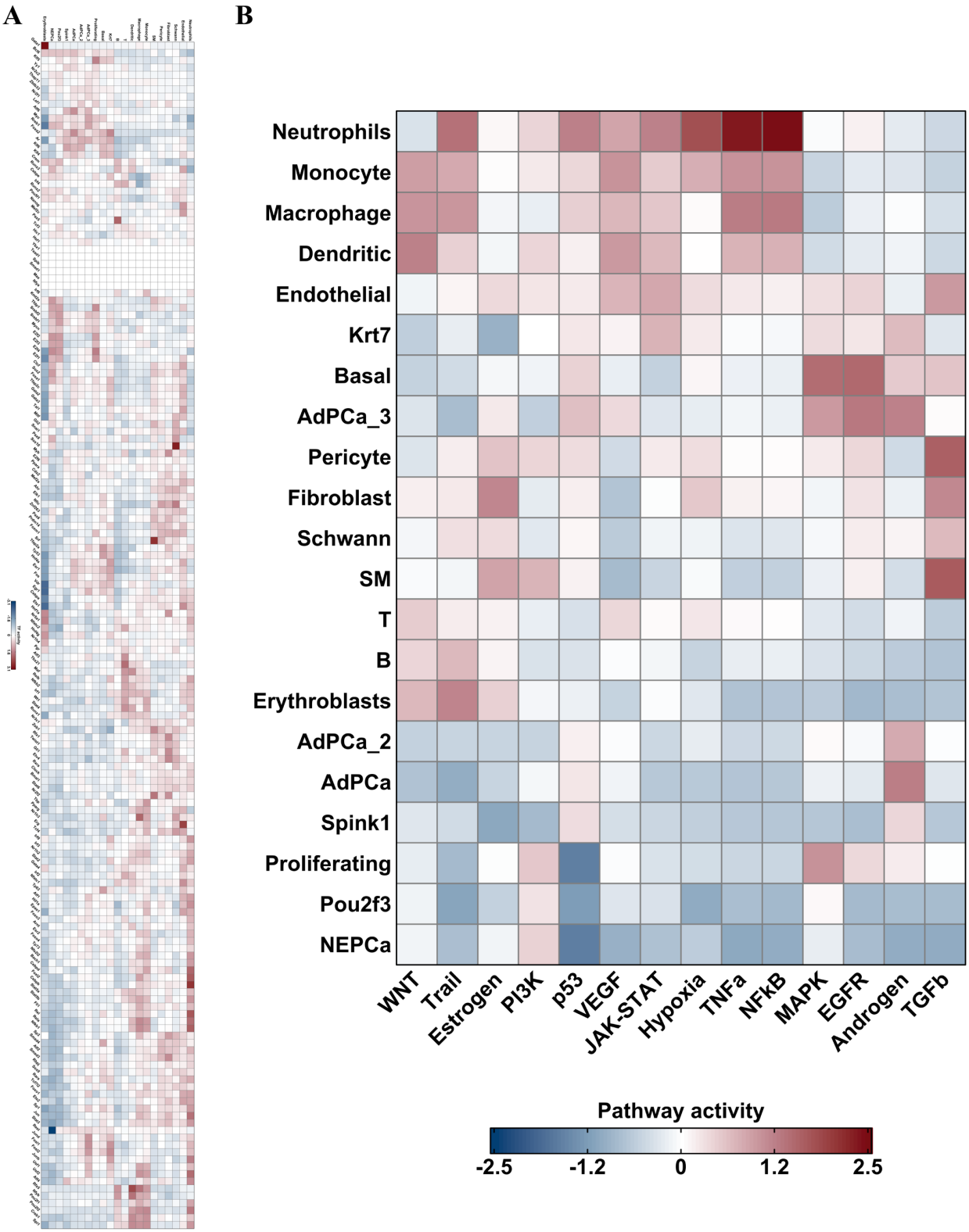

sFig.10: Upstream analysis for MoPSA. Heatmaps were used to visualize the calculated upstream transcription factor activity (A) and signaling pathway analysis for MoPSA.